Wright State University

CORE Scholar

Browse all Theses and Dissertations | Theses and Dissertations

2014

Investigating Anatomical and Molecular Aspects of Proprioceptive Sensory Neuron Diversity using a Transgenic Mouse Model

Martha Jean Sonner
Wright State University

Follow this and additional works at: https://corescholar.libraries.wright.edu/etd_all

 Part of the Neuroscience and Neurobiology Commons, and the Physiology Commons

Repository Citation

Sonner, Martha Jean, "Investigating Anatomical and Molecular Aspects of Proprioceptive Sensory Neuron Diversity using a Transgenic Mouse Model" (2014). *Browse all Theses and Dissertations*. 1253.
https://corescholar.libraries.wright.edu/etd_all/1253

This Thesis is brought to you for free and open access by the Theses and Dissertations at CORE Scholar. It has been accepted for inclusion in Browse all Theses and Dissertations by an authorized administrator of CORE Scholar. For more information, please contact library-corescholar@wright.edu.

INVESTIGATING ANATOMICAL AND MOLECULAR ASPECTS OF PROPRIOCEPTIVE SENSORY NEURON DIVERSITY USING A TRANSGENIC MOUSE MODEL

A thesis submitted in partial fulfillment of the
Requirements for the degree of
Master of Science

By

MARTHA JEAN SONNER
B.S., Ohio Northern University, 2000

2014
Wright State University

WRIGHT STATE UNIVERSITY

GRADUATE SCHOOL

DECEMBER 15, 2014

I HEREBY RECOMMEND THAT THE THESIS PREPARED UNDER MY SUPERVISION BY Martha Jean Sonner ENTITLED Investigating Anatomical and Molecular Aspects of Proprioceptive Sensory Neuron Diversity Using a Transgenic Mouse Model BE ACCEPTED IN PARTIAL FULFILLMENT OF THE REQUIREMENTS FOR THE DEGREE OF Master of Science.

David Ladle, Ph.D.
Thesis Director

Timothy Cope, Ph.D.
Department Chair
Department of Neuroscience, Cell Biology and Physiology

Committee on
Final Examination

Timothy Cope, Ph.D.

Mark Rich, Ph.D.

Robert E. W. Fyffe, Ph.D.
Vice President for Research and
Dean of the Graduate School

ABSTRACT

Sonner, Martha Jean. M.S. Department of Neuroscience, Cell Biology and Physiology, Wright State University, 2014. Investigating Anatomical and Molecular Aspects of Proprioceptive Sensory Neuron Diversity Using a Transgenic Mouse Model.

Muscle spindles (MS) and Golgi tendon organs (GTOs) are encapsulated, stretch-activated sensory receptors housed within skeletal muscles, yet their functional contributions to proprioceptive monitoring of limb movements are quite different. For example, MS are responsible for detecting stretch of muscle fibers, and GTOs provide feedback regarding muscle tension during contraction. Peripheral axons extending from proprioceptive sensory neurons (PSNs) in the dorsal root ganglia supply MS and GTOs. MS are innervated by Group Ia and II sensory fiber endings, while GTOs are innervated by a single Group Ib sensory fiber. The developmental processes guiding axons from PSNs to their targets and the maturation of distinct functional identities in skeletal muscle, however, remain largely unknown. To study PSNs and their peripheral endings more closely, we took advantage of existing transgenic mouse models using Cre-lox recombination technology in which all proprioceptive afferents are labeled with a red fluorescent protein, tdTomato (Parvalbumin-Cre/+; Rosa-CAG-LSL-tdTomato-WPRE). Using this model, we present results from a quantitative confocal microscopy analysis of

proprioceptive receptors and their associated afferent axons taken from whole-mount neonatal mouse soleus muscle preparations.

We focused a portion of our analysis on the unique extramuscular bifurcation of the soleus nerve, which gives rise to stereotypic thin and thick nerve branches. Our results show that the proprioceptor-enriched thin branch of the soleus nerve always contains Ib afferents and usually a mix of Ia and II spindle afferents, but occasionally lacks MS afferents altogether or contains MS afferents of only one type. Heterogeneity in the thin branch may provide a useful tool in analysis of MS and GTO maturation during embryonic and early postnatal development. Additionally, we optimized a technique for retrieving single fluorescently labeled neurons from wild-type and PV-Cre/+; Rosa-tdT/+ dorsal root ganglia and utilized qRT-PCR to screen those neurons for expression of established and putative markers of PSNs.

TABLE OF CONTENTS

TABLE OF CONTENTS (Continued) Page

LIST OF FIGURES

LIST OF FIGURES (Continued) Page

LIST OF TABLES

Table Page

I. INTRODUCTION

Proprioception is the term designated for the body's ability to sense limb position and movement without the aid of visual cues. For example, proprioceptive sensation assists a blindfolded child in accurately swinging a bat and breaking open a piñata, a waitress in tying the strings of her apron behind her back, and a runner in sprinting without needing to look at his feet. In order to perform even the simplest motor tasks, the body requires perpetual monitoring of alterations in muscle length, the amount of force during muscle contraction, joint angle changes, and other biomechanical parameters. Proprioceptive sensory neurons (PSNs) collect this information and relay it to the central nervous system for interpretation and response via spinal circuits and ascending pathways into the brain (Pierrot-Deseilligny and Burke, 2005). Axons extending into the periphery from PSN cell bodies localized in the dorsal root ganglia (DRG), supply specialized sensory receptors located in skeletal muscle, and these proprioceptive receptors are known as muscle spindles (MS) and Golgi tendon organs (GTOs).

This thesis focuses on anatomical and molecular characterization of sensory afferents innervating these peripheral receptors. In many ways, PSNs are similar; however, there are key aspects in which they differ. We hypothesize that one major area of differences exists at the molecular level and thus directs developing PSNs

toward an intrinsically derived structural and functional fate. Much of what is currently known about PSN diversity stems from anatomical, morphological, and physiological properties. In recent years, genetic approaches have also identified a cast of transcription factors and cellular signaling processes that contribute to the development and orchestration of sensory-motor circuitry. Here, we begin by reviewing the current understanding of PSN subclasses according to structural, functional, and molecular perspectives.

Review of Proprioceptive Receptor Structure and Function

MS and GTOs are both encapsulated, stretch-activated sensory receptors housed within skeletal muscles, yet there are several areas in which they are quite different. Anatomically, MS and GTOs are found in different regions of the muscle. MS are located in the belly of the muscle, positioned in parallel with extrafusal muscle fibers, and GTOs are found at myotendinous junctions, arranged in series with muscle fibers. MS and GTOs diverge in their morphological traits as well. In general, MS are comprised of three types of intrafusal muscle fibers (termed bag_1, bag_2, and chain fibers according to nuclear arrangement), a primary afferent ending, variable numbers of secondary afferent endings, and gamma-motor innervation, all surrounded by a capsule structure (Banks, 2005). The primary afferent ending forms the hallmark annulospiral morphology of the MS as it wraps around each type of intrafusal muscle fiber, whereas secondary afferent endings are likened to a spray of flowers and are known to only contact bag_2 and chain intrafusal muscle fibers

(Boyd, 1980). GTOs, on the other hand, are considered to be less complex structurally and are recognized as branching sensory endings that wrap around collagen fibers at the point where muscle meets tendon. Not all muscle fibers feed into GTOs. A typical GTO receives a small group of muscle fibers, which are believed to represent a sampling of the motor units contained within that muscle. (Schoultz and Swett, 1972; Houk et al., 1971; Scott, 2005). Based on ratio calculations performed in cat hind limb experiments, it is thought that the relatively small number of GTOs populating a given muscle is enough to adequately track motor unit activity (Jami, 1992).

Another area in which MS and GTOs differ concerns the types of afferent axons that supply them. Group Ia (primary) and Group II (secondary) afferents have been shown to innervate MS, while Group Ib afferents innervate GTOs (Brown, 1981; Banks, 2005; Scott, 2005). These classifications of afferents are sorted according to traits such as axonal diameter and conduction velocity. For example, in the cat, Ia fiber diameter has been measured in the range of 10 to 22 μm compared to the smaller diameter Group II fibers reported to range from 5 to 14 μm (Zelena, 1994). Because of differences in axonal diameter, expected differences in conduction velocities have also been documented. In the adult cat, Group Ia afferents conduct impulses at a rate of 55 to 120 m/sec, Group Ib afferents from 70 to 110 m/sec, and Group II afferents from 20 to 65 m/sec (Houk and Henneman, 1967; Boyd and Smith, 1984). Data collected from conduction studies in cats indicate Group Ib afferents conduct at velocities quite similar to the Ia afferents such

that they cannot be distinguished on the basis of conduction velocity (Pierrot-Deseilligny and Burke, 2012). In adult mice, Group I afferents (including Ia and Ib) targeting the posterior biceps muscle conducted at 42.9 ± 4.3 m/s on average (± standard deviation) and Group II afferents were reported to average 20.3 ±5.7 m/s (Steffens et al., 2012). It is important to note that, when considered together, these measurements do tend to exhibit some overlapping ranges and therefore classifying muscle afferents according to these properties alone may not render the most accurate results.

In addition to innervating different peripheral targets, Group Ia, Ib, and II afferents have also been shown to differ in their central trajectories and targets. Ia and Ib afferents, for example, are not known to converge on the same interneuronal populations (Eccles et al., 1956). Upon entering the spinal cord via the dorsal root, Ia afferents project to the lamina IX in the ventral horn where they synapse directly onto motoneurons (MNs). In addition, Ia afferents also make connections with populations of interneurons, one of which is known as the Ia inhibitory interneurons, positioned just dorsal to the MN pool (Brown and Fyffe, 1978; Brown, 1981; Jankowska, 1992). Group II spindle afferents also directly contact MNs, although not to the extent of the Ia afferents. Other known central targets of Group II afferents include interneurons located in laminae IV through VII (Brown, 1981; Jankowska, 1992). In contrast, Group Ib afferents do not make monosynaptic connections with MNs. Instead, their central targets include Ib inhibitory

interneurons mainly in lamina VI and occasionally in laminae V and VII (Eccles et al., 1954; Brown and Fyffe, 1979; Brown, 1981; Jankowska, 1992).

Differences in Group Ia, II, and Ib axon fiber types also occur in parallel with differences in the functional profiles of MS and GTOs in the provision of proprioceptive feedback. Upon stretch stimulation, the proprioceptive sensory terminals within MS and GTOs are deformed, which is believed to activate stretch-sensitive ion channels allowing for subsequent influx of sodium, receptor depolarization, and action potential generation (Scott, 2005; Bewick and Banks, 2014). The ion channel(s) responsible for stretch sensitivity of MS and GTOs is yet unknown. In general terms, MS are responsible for detecting changes in muscle length, as evidenced by their increased activity when muscle is stretched and decreased activity during muscle contraction (Hunt and Kuffler, 1951; Hasan and Houk, 1975; Haftel et al., 2004). MS have also been shown to play an important role in muscular responses to changes in body posture (Honeycutt et al., 2012). Furthermore, MS are supplied by both Group Ia and Group II afferents, so it is important to consider the physiological responses of each. For example, during a muscle ramp and hold stretch, Group Ia afferents display marked increases in frequency of action potentials during the ramp phase followed by rapid adaptation at the start of the hold phase of the stretch. On the contrary, Group II afferents show a slower increase in firing during the ramp and much slower adaptation during the hold phase (Jansen and Matthews, 1962; Nicholls et al., 2012). As a result, Group Ia afferents are concluded to be more sensitive to stretch velocity or dynamic stretch,

whereas Group II afferents are mainly sensitive to maintained or static stretch (Mathews, 1981; Nicholls et al., 2012).

While MS are classically understood to oversee length changes in skeletal muscle, GTOs are known for increased activity during active muscle contraction and thus contribute to proprioception through monitoring force of muscle contraction. When a muscle is stretched, or lengthened, a degree of passive tension develops in the muscle. During contraction, however, the resulting tension is deemed to be active. The current understanding is that GTOs are not equally sensitive to passive versus active tension (Jami, 1992). Unfortunately, in the field of proprioception, the MS has commanded greater attention to date than the GTO resulting in limitations in the current knowledge of its physiological contributions. One major finding, from isolating ventral root filaments in adult cats, was that one GTO can report contractile activity from one motor unit (Houk and Henneman, 1967). It is interesting to compare the ratios of numbers GTOs and MS to the numbers of motor units in given muscles. For example, the adult cat soleus is reported have 3.3 motor units for every GTO and 2.8 motor units for every MS. In comparison, the flexor digitorum longus has 9.1 motor units per GTO and 3 motor units per MS. It is postulated that a lower motor unit to GTO ratio may imply more critical monitoring of contractile activity (Eldred et al., 1962; Burke et al., 1977; Jami, 1992).

The above briefly summarizes over 100 years of extensive investigation, and based on this compilation of anatomical and physiological work, it can be confidently concluded that MS and GTOs indeed differ from each other in the

following areas: anatomy and morphology, afferent axon supply, neurocircuitry, and physiological contributions to proprioception. At the center of all of these differences are the unique characteristics of multiple PSN subclasses, currently identified by their associated Group Ia, Ib, and II afferents. The developmental process guiding the growth of axons from these PSNs in the dorsal root ganglia to their specific targets and ultimate functional identities in skeletal muscle, however, remains unknown. In order to further elucidate this developmental process, it is necessary to also study the genetic factors that are involved in neuronal differentiation and axonal guidance, which culminate in neurocircuit formation for the purpose of locomotion.

Review of PSN Molecular Identification

During development, PSNs participate in an intricately choreographed sequence of events, contributing to the construction of neural circuits that unite central and peripheral elements for the purpose of movement. It is not exactly understood how and when PSN subclasses and their pathways to muscle targets are decided. Deductive genetic approaches have brought to light key indicators of PSN identity including the following cytoplasmic and cell surface markers, trophic factors, and regulators of transcription.

As a group, PSNs are known to express the calcium binding protein parvalbumin (PV), which has become a useful tool for immunohistochemical analysis and genetic manipulations of these neurons (Copray et al., 1994; Ernfors et

al., 1994; Honda, 1995; Patel et al., 2003; Hippenmeyer et al., 2005). Initial experiments with cultured embryonic rat DRG neurons demonstrated that the population of neurons that relied most on NT3 for survival also largely expressed PV. It was also shown that this population of neurons tended to be cells with large soma diameters (Copray et al., 1994). Retrograde nerve fills of the sural and gastrocnemius nerves subsequently linked PV expression to muscle, but not cutaneous afferents (Honda, 1995). PV is also widely used in labeling PSNs via immunofluorescence. For example, PV immunostaining was used to confirm the complete loss of PSNs in the DRG of a $NT3^{-/-}$ mouse model compared to control mice (Ernfors et al., 1994). With the generation of PV-Cre driver mice came the ability selectively manipulate the PSN population genetically (Hippenmeyer et al., 2005). For instance, PV-Cre expressing mice have been used to selectively knock out the synaptic vesicle associated protein, munc18-1, in PSNs and effectively block their synaptic transmission (Dallman and Ladle, 2013). Although all PSNs express PV, PV expression is not strictly limited to PSNs. Cutaneous mechanoreceptors supplying Pacinian, Meissner, and Lanceolate endings also express PV; therefore, PV expression with co-expression of other positive markers has been used to unequivocally identify PSNs (de Nooij et al., 2013).

It has also been well established that all PSNs require neurotrophin 3 (NT3) for cell survival. NT3 knock-out mice exhibit substantial loss of DRG neurons as well as a complete lack of MS and GTOs within skeletal muscles (Ernfors et al., 1994). When transgenic mice overexpressing NT3 in skeletal muscles were bred with NT3

knock-out mice, a portion of Group Ia afferents and MS were rescued in the offspring (Wright et al., 1997). Additionally, in mice where tyrosine kinase receptor C (TrkC), the receptor for NT3, had been knocked out, 19% of DRG neurons were lost, Ia and II afferents were not observed in the spinal cord and dorsal roots, and the animals exhibited behavioral phenotypes consistent with proprioceptive deficits (Klein et al., 1994). Conversely, when NT3 was genetically overexpressed in skeletal muscle, there was also an increase in the number of PSNs and, in turn, MS counts elevated up to 300% in some muscles (Wright et al., 1997). TrkC expression thus serves as a molecular marker for PSNs, and NT3 signaling is an effective way to genetically manipulate the PSN population.

One aspect that contributes to the molecular identity of PSNs deals with establishing central patterns of connectivity. Er81 is a transcription factor that depends on peripheral NT3 for induction and is required for correct formation of Ia afferent monosynaptic connections onto MNs during development (Arber et al., 2000; Patel et al., 2003). Er81 knock-out mice revealed several important consequences. Although PSNs are present, their central trajectories are halted in the intermediate zone, and the monosynaptic input of spindle afferents onto MNs is lost (Arber et al., 2000). MS started to develop normally embryonically, but by P5, intrafusal muscle fibers failed to differentiate, complicating the formation of the annulospiral morphology, and markedly reducing MS response to muscle stretch (Arber et al., 2000). Interestingly, spindle sensory ending loss among PSNs is not uniform in all muscles after the loss of Er81. PSNs supplying spindle endings within

proximal muscles were more severely affected than those supplying more distal muscles, suggesting that muscle target specificity is an important factor to consider when comparing PSNs molecularly (Kucera et al., 2002; de Nooij et al., 2013).

In addition to Er81, Runx3 is another transcription factor necessary for the establishment of connections between PSNs and their central terminations. Experiments utilizing a Runx3 knock-out mouse model revealed a marked ataxic phenotype, quite similar to the phenotypic behaviors elicited in $TrkC^{-/-}$, $NT3^{-/-}$, and $Er81^{-/-}$ mice (Chen, et al., 2003). In the Runx3 mutant, observed proprioceptive deficits were linked to PSN absence in the DRGs, loss of Group Ia monosynaptic input onto MNs, and lack of MS in skeletal muscles (Inoue et al., 2002; Levanon et al., 2002). PV staining showed a decreased number of PSNs in the DRG and proprioceptive afferents were lacking in both the ventral horn and intermediate zone of the spinal cord. Manipulation of Runx3 expression levels in chick embryos suggested that higher levels of Runx3 direct proprioceptive axons to the ventral horn while lower levels of Runx3 cause axons to terminate more dorsally in the intermediate zone (Chen et al., 2006). Taken together, TrkC, PV, Er81, and Runx3 mutual expression is used to molecularly detect the PSN population (de Nooij et al., 2013).

Currently, this level of resolution is the extent to which PSNs can be molecularly identified. Selective markers for subsets of PSNs associated with Group Ia, Ib, and II afferents have not yet been uncovered. We hypothesize that genetic differences exist between the subpopulations of PSNs that project axons to MS

versus those that project to GTOs. If authentic, these cell intrinsic distinctions could have the potential to be deciding factors in the development of the unique structural and functional properties that define these two proprioceptive receptor classes. Genetic manipulation of subsets of PSNs would indeed provide an avenue for many novel experimental endeavors expanding our understanding of the development of proprioception, monitoring the regrowth of proprioceptive afferents following peripheral nerve injury, and studying the mechanisms underlying peripheral neuropathy, to suggest a few. Here, we present three aims to test our hypothesis. First, we sought to develop and assess a technique that would allow us to quantify MS and GTOs in a whole-mount muscle preparation from a transgenic mouse. Next, we wanted to determine if a whole-mount muscle preparation would enable us to predict the number of PSNs projecting to the mouse soleus by analyzing the proprioceptive axons supplying each MS and GTO. Finally, we aimed to capture single fluorescently labeled cells from DRGs and perform qRT-PCR to screen for differential gene expression among subclasses of PSNs. If successful, this project could serve as the foundation for future inquiries into the diversity and development of PSNs.

II. MATERIALS AND METHODS

All animal experimental procedures were conducted under the approval of the Wright State University Laboratory Animal Care and Use Committee.

Transgenic Animal Model for Labeling Proprioceptive Afferents

Knock-in transgenic mice expressing Cre-recombinase from the parvalbumin locus (Hippenmeyer, et el., 2005; PV-Cre, C57 background, JAX Stock 008069) were crossed with fluorescent reporter mice to allow visualization of PSNs and their peripheral endings in a whole-mount muscle preparation. The reporter mice contained a lox-STOP-lox cassette upstream of a tdTomato red fluorescent protein inserted into the Rosa26 locus, which is highly expressed in all mouse tissues. (Rosa-tdT/+; JAX Stock 007908). In this case, Cre-mediated recombination produced a phenotype in which all PSNs, including cell bodies, afferent axons, and respective terminations within skeletal muscle are labeled with a red fluorescent protein.

Soleus Muscle Collection for Immunohistochemistry

At age P3, a PV-Cre/+; Rosa-tdT/+ mouse was anesthetized via hypothermia induced from an ice-water bath and transcardially perfused with 10 mL of ice-cold 1X PBS followed by 10 mL of 4% paraformaldehyde (PFA) solution. All musculature superficial to the soleus muscle (hamstrings, lateral and medial gastrocnemius muscles) was removed from the right hind limb, and the soleus nerve was cut proximal to the point where the thin branch defasciculates. The entire lower hind limb, including exposed soleus muscle, was then submerged in 15 mL of 4% PFA for 1 hour at 4°C. After fixation, the lower hind limb was washed two times with 1X PBS and then placed in 15 mL of 30% sucrose solution overnight at 4°C for cryoprotection. The soleus muscle was then removed from the limb, embedded in tissue freezing medium and placed in a freezer at -80°C. Using a HM 550 cryostat, 20 μm-thick serial longitudinal sections were obtained and placed on Superfrost Plus microscope slides in preparation for immunohistochemistry. The soleus muscle sections were washed two times with 1X PBS and then incubated overnight at 4°C in a primary antibody solution containing: Guinea pig anti-VGLUT1 Polyclonal Antibody diluted 1:10,000 (Chemicon AB5905, Lot LV1567574), 1X PBS, 1% bovine serum albumin, and 0.3% Triton X-100. The sections were next washed three times with 1X PBS and then incubated for 45 minutes, protected from light, at 22°C in a secondary antibody solution containing: 2 mg/mL Alexa Fluor® 488 Goat Anti-Guinea Pig IgG (H+L) Antibody diluted 1:1000 (Invitrogen A11073, Lot 455283), 1X PBS, 1% bovine serum albumin, and 0.3% Triton X-1000. Following the secondary

incubation, the sections were washed three times with 1X PBS. Vectashield® mounting medium (H-1000, Vector Laboratories, Inc.) was then applied to the sections for fluorescence preservation prior to placement of a 22 x 50 mm glass coverslip. High magnification images (60X) of proprioceptive receptors and afferent axons were acquired using an Olympus FV1000 confocal microscope.

Quantification of Proprioceptive Receptors in the Mouse Soleus Muscle

Fifteen PV-Cre/+; Rosa-tdT/+ mice, ages P3 to P7 were anesthetized via hypothermia induced from an ice water bath and transcardially perfused with 5 mL of ice-cold 1X PBS in preparation for muscle retrieval. The animal preparations were then submerged in ice-cold 1X PBS for the remaining duration of the dissection. The soleus muscle and nerve were quickly isolated and removed from the right hind limb and mounted on a 25 x 75 mm, 1.0 mm thick glass slide with a drop of 1X PBS. Adapting a technique described by Vult von Steyern, a 22 x 50 mm glass coverslip was next applied to compress the muscle to a thickness optimal for documentation of proprioceptive axons and their associated endings using fluorescence microscopy (Vult von Steyern et al., 1999). Images were immediately acquired using an Olympus BX51 Epi Fluorescence microscope (4x and 10x) with SPOT RT Slider 2.3.0 color camera and SPOT Advanced software version 5.1 (Diagnostic Instruments, Inc.). The number of MS and GTOs contained within the soleus muscle were quantified using known morphological characteristics, namely the hallmark annulospiral structure of muscle spindles and the flower spray

arrangement of Golgi tendon organs (Boyd, 1980). Furthermore, careful attention was paid to whether proprioceptive axons supplying a given MS or GTO reached the ending via the soleus nerve thick branch, thin branch, or both. Throughout the data analysis, averages were reported as mean ± SEM.

Analysis of Proprioceptive Sensory Axons Supplying Sensory Endings in the Mouse Soleus Muscle

Four PV-Cre/+; Rosa-tdT/+ mice, ages P3 to P5 were anesthetized via hypothermia induced from an ice water bath and transcardially perfused with 5 mL of ice-cold oxygenated (95% O_2; 5% CO_2) artificial cerebrospinal fluid (ACSF) containing: 127 mM NaCl, 1.9 mM KCl, 1.2 mM KH_2PO_4, 1 mM $MgSO_4 \cdot 7H_2O$, 26 mM $NaHCO_3$, 16.9 mM D(+)-glucose monohydrate, and 2 mM $CaCl_2$. Here, the soleus muscle dissection was performed with the animal preparation submerged in a recirculating bath of cold oxygenated ACSF. Following excision, the soleus muscle was carefully pressed between two glass slides, each prepared with a layer of filter paper and 40 μm cell strainer mesh, and then secured together with adhesive tape. This entire compression apparatus was immediately submerged in 40 mL of 4% PFA solution for 1 hour at 4°C. In this manner, muscle compression and fixation were accomplished simultaneously as the filter paper wicked the PFA in between the two slides while the cell strainer mesh provided a PFA-accessible yet non-traumatic protective covering for the soleus muscle. After fixation, the compressed soleus muscle was rinsed three times with 1X PBS, mounted on a Superfrost Plus

microscope slide with Vectashield mounting medium, and a 20 x 50 mm glass coverslip.

In order to document the number of proprioceptive axons supplying a subset of representative soleus spindles and GTOs, images (20X and 60X) of the compressed and fixed muscles were acquired and analyzed using an Olympus FV300 confocal microscope in conjunction with Fluoview software. Composite images were constructed in Photoshop (CS3) from maximal intensity projections from confocal images. Counts of proprioceptive axons were performed with the assistance of 3D image visualization software as needed (Imaris 7.7.0).

Proprioceptive Sensory Neuron Labeling Via Retrograde Peripheral Nerve Fill

Five mice (*n* = 3 wild type; *n* = 2 PV-Cre/+; Rosa-tdT/+) ages P4-P5 were anesthetized via hypothermia induced from an ice water bath and transcardially perfused with 5 mL of ice-cold oxygenated ACSF. For these experiments, 5 mL of Penicillin-Streptomycin solution (5,000 IU/mL and 5mg/mL, respectively) was included in the ACSF to prevent microbial growth. As described above, these dissections were also performed with the animal preparation submerged in a recirculating bath of cold, oxygenated ACSF. To allow for optimal oxygenation of PSNs housed within the dorsal root ganglia, we performed a dorsal laminectomy and released the dura from the spinal cord along the entire length of the spinal column. All ventral roots were cut bilaterally to prevent muscle contraction. Dorsal roots at lumbar segments 1 through 5 on the animal's right side remained intact; all

other ipsilateral and contralateral dorsal roots were cut. The quadriceps nerve was then carefully isolated and transected, and the proximal portion of the nerve was drawn up in to a fire-polished glass capillary tube (TW120F-4, World Precision Instruments, Inc.). Once the cut nerve was well seated within the capillary glass, ACSF remaining in the capillary was removed, and 2 μL of fluorescent dextran solution was injected into the capillary glass to allow for retrograde transport overnight (approximately 16 hours) at 22°C to the cell bodies contained within DRG-L3 and DRG-L4. Tetramethylrhodamine Dextran, 3000 MW, Anionic, Lysine Fixable (100 ng/mL, Invitrogen D-3308) was used to fill the quadriceps nerve in wild type (WT) animals, while Fluorescein Dextran, 3000 MW, Anionic, Lysine Fixable (100 ng/mL, Invitrogen D-3306) was used in PV-Cre/+; Rosa-tdT/+ animals.

Prior to performing the retrograde quadriceps nerve fill experiments, a pilot experiment was conducted using methods described, however, using a P4 PV-Cre/+; Rosa-tdT/+ peroneal nerve. The peroneal nerve innervates the anterior compartment of the distal hind limb, and sensory neurons sending axons through this nerve are found in DRG-L4 and DRG-L5.

Proprioceptive Sensory Neuron Single-Cell Capture and qRT-PCR

Immediately following successful completion of retrograde nerve fill, WT and PV-Cre/+; Rosa-tdT/+ DRG-L3 and DRG-L4 were carefully removed from the animal preparation and embedded in 1.6% agar. The embedded DRGs were immediately submerged and maintained in partially frozen, oxygenated ACSF while sectioned

into 200 μm-thick slices using a Vibratome® 1000 Plus Sectioning System. The DRG slices were then incubated in oxygenated ACSF for 1 hour at 27°C. Following incubation, the DRG slices were secured in a Sylguard perfusion chamber and maintained in a recirculating bath of oxygenated ACSF at room temperature during single-cell retrieval. Single fluorescently labeled cells were visualized and retrieved from DRG slices using an Olympus 2-Photon microscope (FV-1200MPE) at 25X magnification. Cell retrieval pipettes were prepared from capillary glass (TW150F-3, World Precision Instruments, Inc.) pulled to 20 μm tip diameter using a Narishige PP-830 vertical pipette puller and preloaded with 10 to 20 μL of ACSF containing 0.5% Fluorescein Dextran, 250kD (100 ng/μL, Sigma FD250S-100MG). The fluorescent dye aided in initially visualizing the cell retrieval pipette under the objective lens, and this volume was largely expelled from the tip of the pipette during navigation to the DRG slices. Using a Sutter MP-285 motorized micromanipulator, the pipette was positioned to be in direct contact to the cell of interest, negative pressure was carefully applied, drawing the cell of interest into the tip of the retrieval pipette. In all, 14 samples were obtained. Of that total, 7 quadriceps sensory neurons labeled by retrograde fill were collected from three WT mice. In addition, 5 fluorescently indicated PSNs and 1 fluorescently indicated non-PSN (to serve as the qRT-PCR calibrator sample) were collected from two PV-Cre/+; Rosa-tdT/+ mice. Finally, 1 sample, which contained only the 0.5% Fluorescein Dextran solution, served as a negative control.

The Ambion® Single Cell-to-CT™ Kit and accompanying protocol (Life Technologies 4458237) were utilized for single-cell qRT-PCR. Upon retrieval, the single cell was immediately ejected into a DNAse/RNAse-free PCR tube containing 9 µL of Single Cell Lysis Solution and 1 µL of Single Cell DNAse I (prepared on ice) to lyse the cell and remove all DNA material. After incubation for 5 minutes at room temperature, 1 µL of Single Cell Stop Solution was added, and the sample tube was incubated for 2 minutes at room temperature. Stopped cell lysates were stored in a -80°C freezer for 6 to 38 days until batch qRT-PCR was performed. Dr. Michael Markey, Director of the Center for Genomics Research at Wright State University, performed the reactions described next. A reverse transcription reaction mix composed of 3.0 µL of Single Cell VILO™ RT Mix and 1.5 µL Single SuperScript® RT was added to each sample tube. Reverse transcription to obtain cDNA was performed in an Eppendorf Mastercycler as follows: 25°C for 10 minutes; 42°C for 60 minutes; 85°C for 5 minutes. Next, mouse TaqMan® Gene Expression Assays for targets of interest (Life Technologies, see Table 1) were combined and diluted with 1X TE Buffer (pH 8.0) such that the final concentration for each assay was 0.2X. A preamplification reaction mix, consisting of 5 µL of Single Cell PreAmp Mix and 6 µL of the 0.2X combined TaqMan® Gene Expression Assays, was added to each cDNA sample. Preamplification was then carried out in the thermalcycler as follows: 95°C for 10 minutes; 95°C for 15 seconds, 60°C for 4 minutes, repeated 14 cycles; 99°C for 10 minutes. The purpose of this preamplification step was to generate enough material to be sufficient input for qRT-PCR. Preamplification products were diluted

Table 1. TaqMan® Gene Expression Assays (Life Technologies) selected for single-cell qRT-PCR.

Gene	Description	Assay ID
Isl1	ISL1 transcription factor, Lim/homeodomain	Mm00517585_m1
Pvalb	Parvalbumin	Mm00443100_m1
Runx3	Runt related transcription factor 3	Mm00490666_m1
Grm3	Glutamate receptor, metabotropic 3	Mm00725298_m1
Pth1r	Parathyroid hormone 1 receptor	Mm00441046_m1
Esrrg	Estrogen-related receptor gamma	Mm01314576_m1
Gabrg1	Gamma-aminobutyric acid (GABA) A receptor, subunit gamma 1	Mm00439047_m1
Stac2	SH3 and cysteine rich domain 2	Mm00524631_m1
GAPDH	Glyceraldehyde-3-phosphate dehydrogenase (endogenous control)	Mm99999915_g1

1:20 with 1X TE Buffer (pH 8.0) in preparation for qRT-PCR. Using a 96-well plate, each qRT-PCR reaction was performed in triplicate, and each reaction contained the following: 12.5 µL of 2X TaqMan® Gene Expression Master Mix, 5 µL preamplified product diluted 1:20, 1.25 µL of 20X TaqMan® Gene Expression Assay for GAPDH (endogenous control), 1.25 µL of 20X TaqMan® Gene Expression Assay for target of interest, and 5 µL of nuclease-free water. The reactions were measured using an ABI Prism® 7900HT Sequence Detection System (Applied Biosystems) with the following conditions: 50°C for 2 minutes; 95°C for 10 minutes; 95°C for 5 seconds, 60°C for 1 minute, repeated for 40 cycles. Amplification data and relative gene expression results were collected and analyzed using SDS 2.4 and SDS RQ Manager software.

III. RESULTS

Assessment of Transgenic Animal Model

The first aim of this project was to devise and test a method that would enable us to analyze PSNs, their peripheral axons, and their endings in a whole muscle preparation. PSNs are well known to express the calcium binding protein parvalbumin (Copray et al., 1994; Emfors et al., 1994; Honda, 1995; Patel et al., 2003). We therefore employed the cre-lox system of recombination in existing transgenic mouse models to produce PV-Cre/+; Rosa-tdT/+ mice in which all parvabumin-expressing neurons, namely PSNs, are labeled with a red fluorescent protein (Hippenmeyer et al., 2005). It should be noted that as we observed the PV-Cre/+; Rosa-tdT/+ mice at various postnatal ages, it became apparent that, in addition to PSNs, extrafusal muscle fibers also express parvalbumin as early as P0. By P7, nearly all muscle fibers displayed intense tdTomato fluorescence, at which point afferent labeling could no longer be discerned. Consequently, this factor limited our analysis to ages up to P7.

To test the accuracy of this transgenic labeling strategy, we compared immunoreactivity for vesicular glutamate transporter 1 (VGLUT1) to the native

fluorescence of proprioceptive receptors in the PV-Cre/+; Rosa-tdT/+ neonatal mouse soleus (Wu et al., 2004). We compared the native tdTomato fluorescence with antibody staining for VGLUT1 in the soleus muscle at age P3 and observed consistent overlap in both MS and GTOs as shown in Figure 1. Representative confocal images show that VGLUT1 expression was largely restricted to the hallmark annulospiral structure of the MS and the flower-spray structure of the GTO as previously reported (Wu et al., 2004; de Nooij et al., 2013). Expression of the tdTomato reporter was visualized in proprioceptive endings as well as axons. These results confirm the accuracy or our genetic approach for labeling MS and GTOs in the neonatal mouse soleus.

Quantification of Proprioceptive Receptors in the Mouse Soleus Muscle

With our genetic labeling strategy in place, we next sought to quantify the numbers and distribution of MS and GTOs contained within the intact soleus muscle. A consistent characteristic of innervation of the soleus muscle is the presence of thin and thick branches of the common soleus nerve, which diverge prior to muscle entry (Figure 2). The thin branch only supplies sensory endings housed within the proximal compartment of the muscle, while the thick branch provides both sensory and motor innervation to the remainder of the muscle (Vult von Steyern, 1999). Compressing live soleus muscle tissue between a glass slide and coverslip allowed us to rapidly document MS and GTO counts in the entire soleus as well as to determine whether a given proprioceptor was supplied axons via the thick branch,

Figure 1. **The PV-Cre/+; Rosa-tdT/+ transgenic mouse model accurately labeled MS and GTOs in the neonatal mouse soleus.** Examples of native tdTomato fluorescence in a MS **(A – C)** and in a GTO **(D – F)** compared to VGLUT1 antibody stain. Note that VGLUT1 expression was largely restricted to the proprioceptive receptor terminals, while parvalbumin expression was observed in both proprioceptive receptor terminals and axons. Scale bars represent 50 μm.

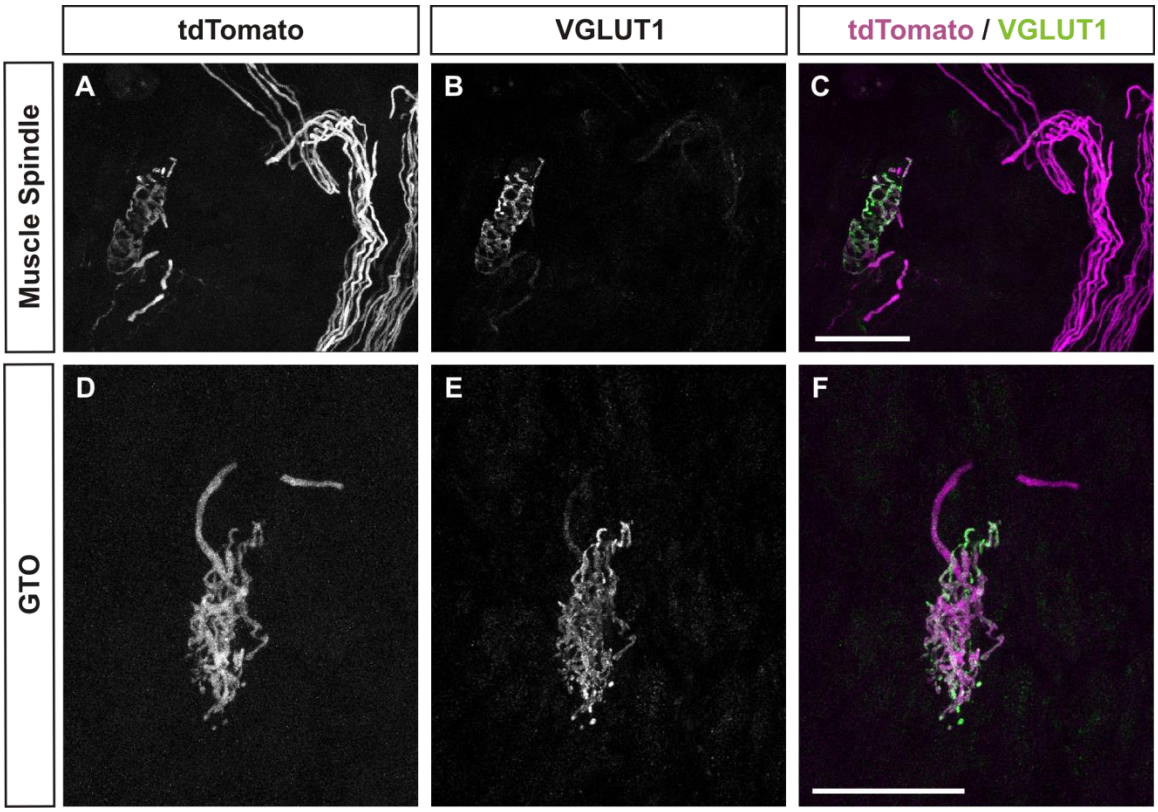
tdTomato
VGLUT1
tdTomato / VGLUT1
Muscle Spindle
GTO
A
B
C
D
E
F

Figure 2. The soleus muscle offered a unique setting for the study of proprioceptors. (A) Schematic representation of the extramuscular bifurcation of the soleus nerve in to thin and thick branches and the distribution of MS and GTOs within the muscle. **(B)** Example of fluorescently labeled proprioceptive afferents and terminals observed in a PV-Cre/+; Rosa-tdT/+ mouse at age P5 using the compressed muscle preparation (4x wide-field image).

A

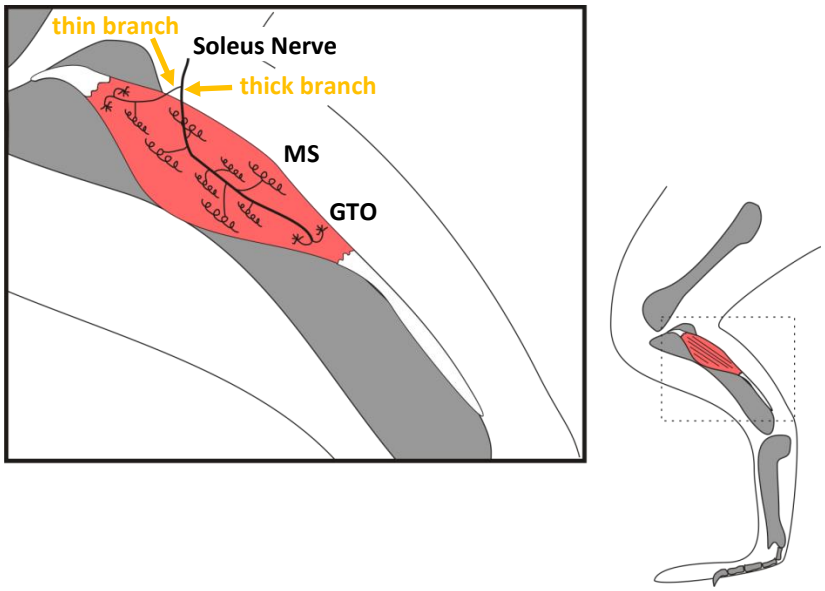
thin branch
Soleus Nerve
thick branch
MS
GTO

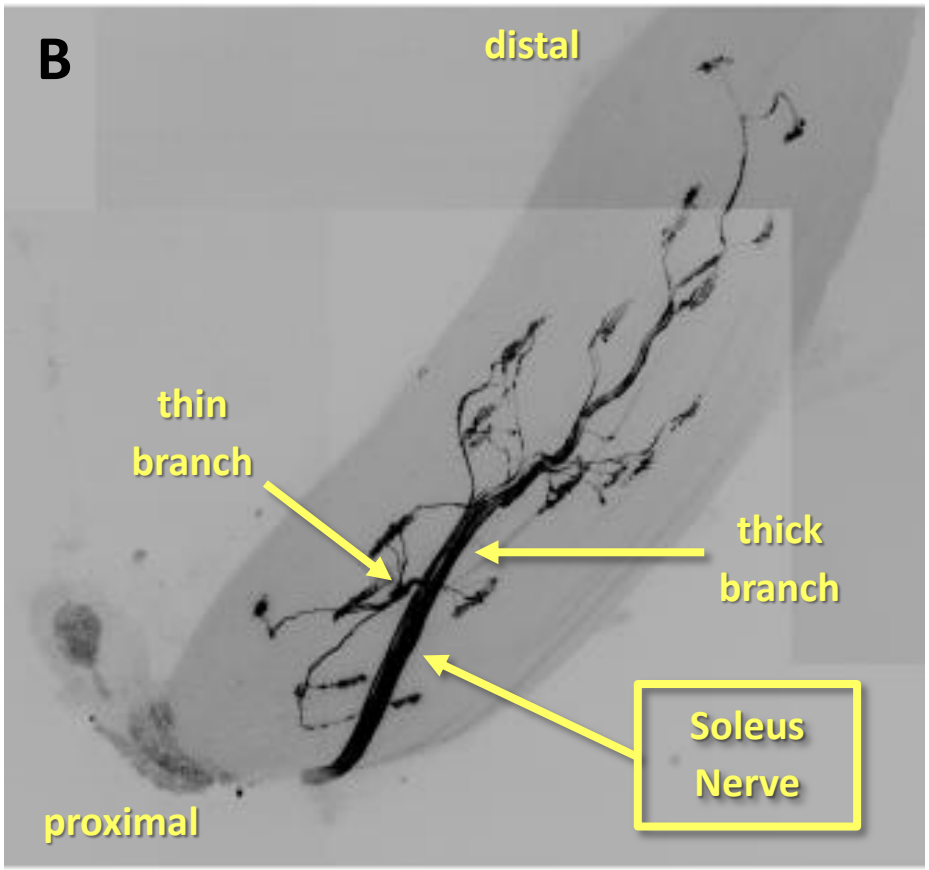
B
distal
thin
branch
thick
branch
Soleus
Nerve
proximal

the thin branch, or both. Our survey of 19 PV-Cre/+; Rosa-tdT/+ mice ages P3 to P7 found the right soleus muscle to contain 10.8 ± 0.3 MS and 5.2 ± 0.2 GTOs (data reported as mean ± SEM; Figure 3A). Our MS counts for the soleus muscle are consistent with other murine MS counts reported previously from data collected from serial sections (Tourtellotte et al., 2001; Patel et al., 2003; Lionikas et al., 2013).

Given the individual variability we observed in the numbers of MS and GTOs contained within the whole soleus nerve, we asked whether above average MS counts were linked to below average GTO counts. Our data suggests that this is not the case (Figure 3B). Animals with above average total MS counts still tended to have GTOs either equal to or above our calculated average number of GTOs. Animals with below average MS counts still maintained the average number of GTOs. Likewise, above average GTO counts did not necessarily indicate fewer MS, and fewer GTOs did not appear to indicate elevated MS. In summary, our analysis showed that numbers of MS and GTOs in the soleus muscle vary independently.

When we focused our analysis on just the thin branch of the soleus nerve, our results revealed the following subset of proprioceptors, namely 1.7 ± 0.2 MS and 2.8 ± 0.8 GTOs (Figure 3C). Again, our results are in close agreement with results presented by Tourtellotte et al., 2001. Interestingly, 6 of the 19 mice studied (31.6%), contained a MS located in the proximal compartment of the soleus muscle innervated by sensory axons from both the thick and thin branches of the soleus nerve. Taken together, the results of these experiments show that the PV-Cre/+;

Figure 3. Quantitative analysis of proprioceptive receptors within the soleus muscle. The PV-Cre/+; Rosa-tdT/+ transgenic mouse model provided ease of identifying and quantifying proprioceptive receptors in a whole-mount soleus muscle preparation at early postnatal ages. **(A)** Our survey of 19 mice ages P3 to P7 found the right soleus muscle to contain 10.8 ± 0.3 MS and 5.2 ± 0.2 GTOs (mean ± SEM). **(B)** Proprioceptive receptor class populations within the mouse soleus appeared to vary independently. Above average total MS counts were not found to occur at the expense of total numbers of GTOs. Below average MS counts occurred along with average or above average GTO counts. Likewise, above average GTO counts did not necessarily indicate fewer MS. Fewer GTOs did not result in elevated MS. **(C)** Our results further showed that the thin branch of the soleus nerve supplies 1.7 ± 0.2 MS and 2.8 ± 0.8 GTOs.

A

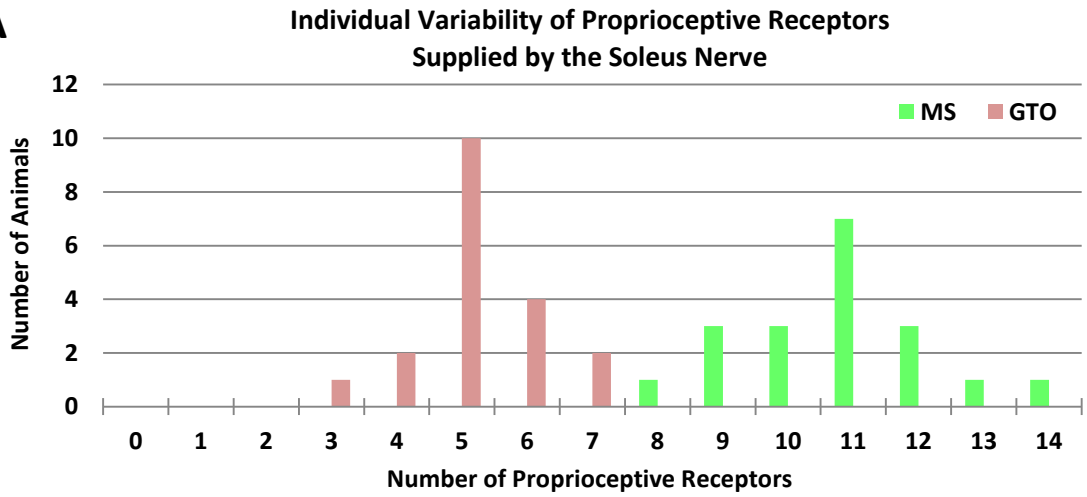
Individual Variability of Proprioceptive Receptors
Supplied by the Soleus Nerve
MS
GTO
Number of Animals
0
2
4
6
8
10
12
0 1 2 3 4 5 6 7 8 9 10 11 12 13 14
Number of Proprioceptive Receptors

B

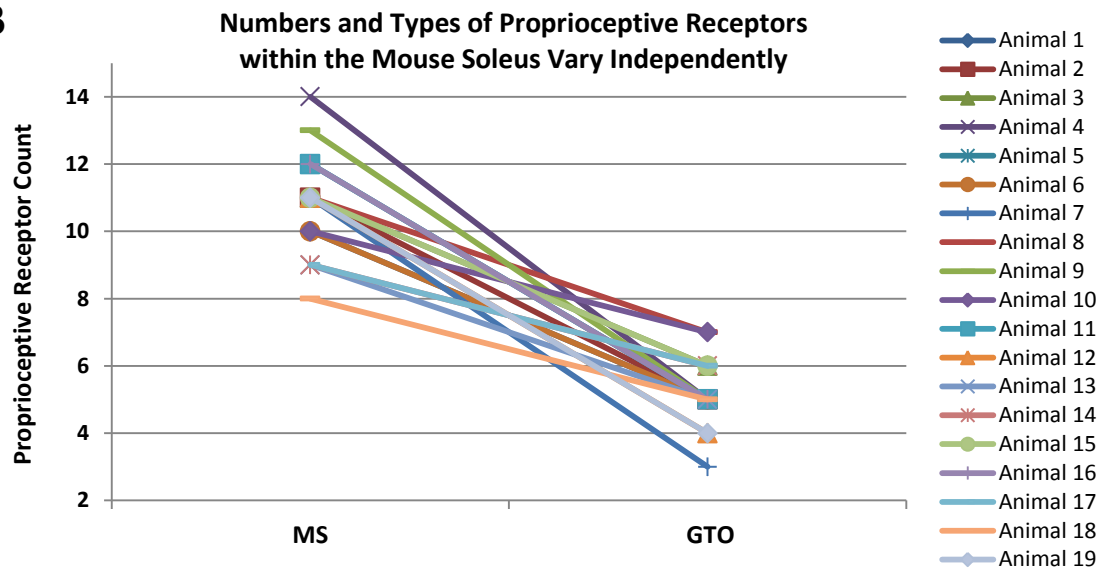
Numbers and Types of Proprioceptive Receptors
within the Mouse Soleus Vary Independently
Proprioceptive Receptor Count
2
4
6
8
10
12
14
MS
GTO
Animal 1
Animal 2
Animal 3
Animal 4
Animal 5
Animal 6
Animal 7
Animal 8
Animal 9
Animal 10
Animal 11
Animal 12
Animal 13
Animal 14
Animal 15
Animal 16
Animal 17
Animal 18
Animal 19

C

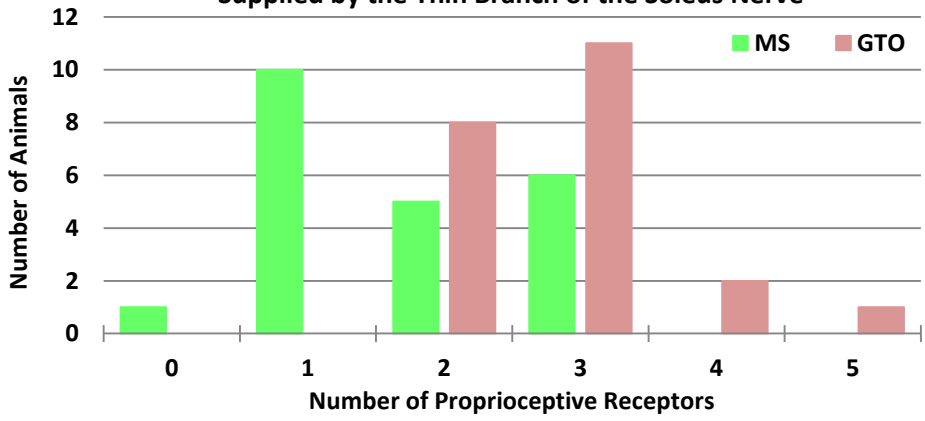
Individual Variability of Proprioceptive Receptors
Supplied by the Thin Branch of the Soleus Nerve
MS
GTO
Number of Animals
0
2
4
6
8
10
12
0 1 2 3 4 5
Number of Proprioceptive Receptors

Rosa-tdT/+ transgenic mouse model is an accurate method of labeling proprioceptive receptors in the intact soleus muscle at early postnatal ages.

Analysis of Proprioceptive Sensory Axons in the Mouse Soleus Muscle

The second aim of the project was to determine the number of PSNs that project to the soleus muscle by analyzing the numbers of axons supplying each proprioceptive receptor at higher magnification. Using 4 PV-Cre/+; Rosa-tdT/+ mice ages P3 to P5, we again employed the soleus muscle compression technique, but also added a brief 4% PFA fixation step to the process. The native fluorescence of the transgenic animals was well preserved through the fixation and prevented degradation of the sensory endings. We imaged each muscle preparation at two levels of magnification with confocal imaging. First, we scanned the entire muscle at 20X and generated composite images to serve as a general map of the proprioceptive innervation (Figures 4, 6, 8, and 10). Second, we scanned a subset of MS, GTOs, and their associated afferents at 60X to obtain detailed maps that represent the diversity in the numbers of axons supplying a given proprioceptive receptor in the mouse soleus (Figures 5, 7, 9, and 11). In total, the 4 muscles analyzed in these experiments contained 40 MS and 20 GTOs. We excluded 1 spindle from our analysis due to axonal damage during preparation.

Figure 4. Animal 1: composite 20X image of proprioceptive innervation within the soleus muscle. Representative MS (green boxes) and GTOs (pink boxes) were selected for high magnification confocal imaging and analysis.

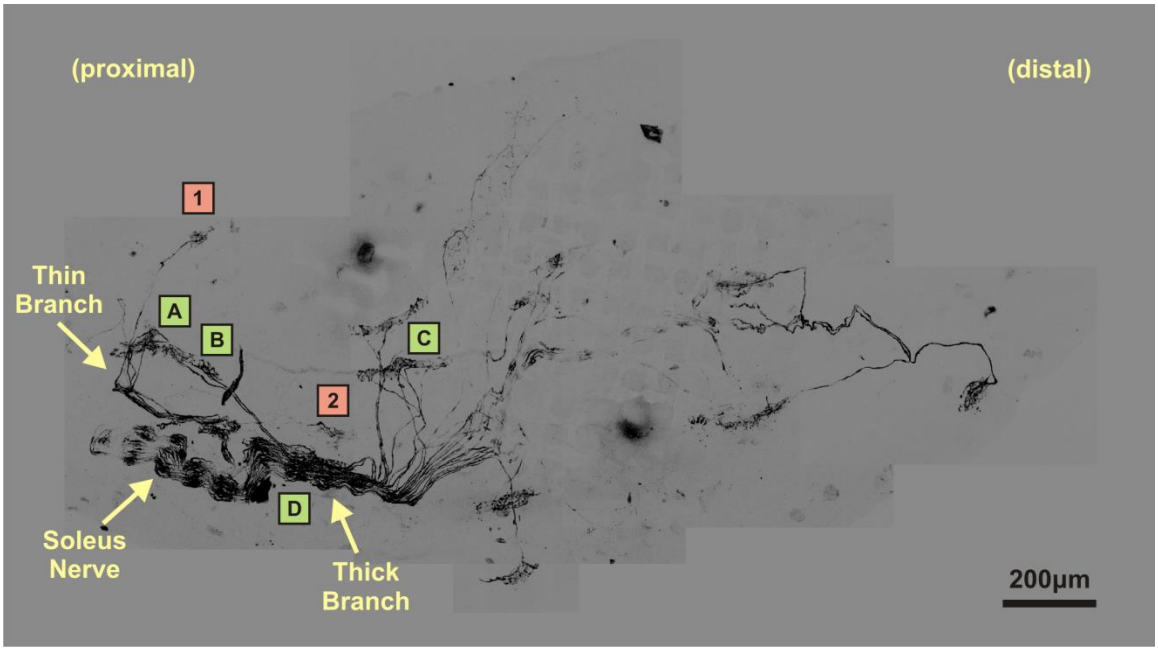
(proximal)
(distal)
1
Thin
Branch
A
B
C
2
D
Soleus
Nerve
Thick
Branch
200µm

Figure 5. Animal 1: composite 60X images of representative MS (green boxes), and GTOs (pink boxes). (A and C) GTO 1 and GTO 2, each supplied by a single Ib axon via the thin branch of the soleus nerve. **(B)** Spindle A, supplied by two proprioceptive axons via the thin branch of the soleus nerve. **(D)** Spindle B with three associated proprioceptive axons, two via the thick branch and one via the thin branch. **(E)** Spindle C with three associated proprioceptive axons all supplied via the thick branch. **(F)** Spindle D with four associated proprioceptive axons, three via the thick branch and one via the thin branch.

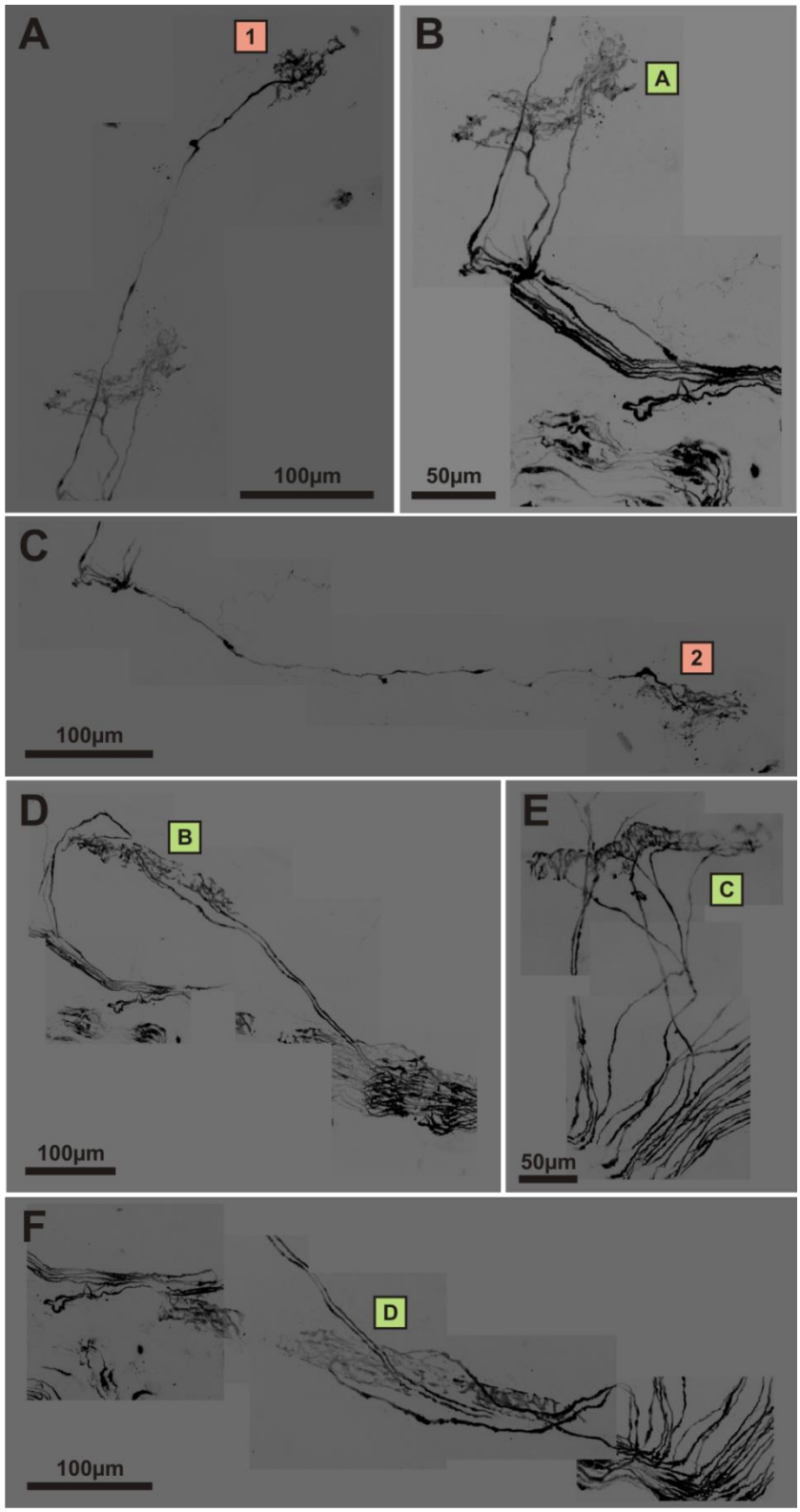
A
1
100µm
B
A
50µm
C
2
100µm
D
B
100µm
E
C
50µm
F
D
100µm

Figure 6. Animal 2: composite 20X image of proprioceptive innervation within the soleus muscle. Representative MS (green boxes) and GTOs (pink boxes) were selected for high magnification confocal imaging and analysis.

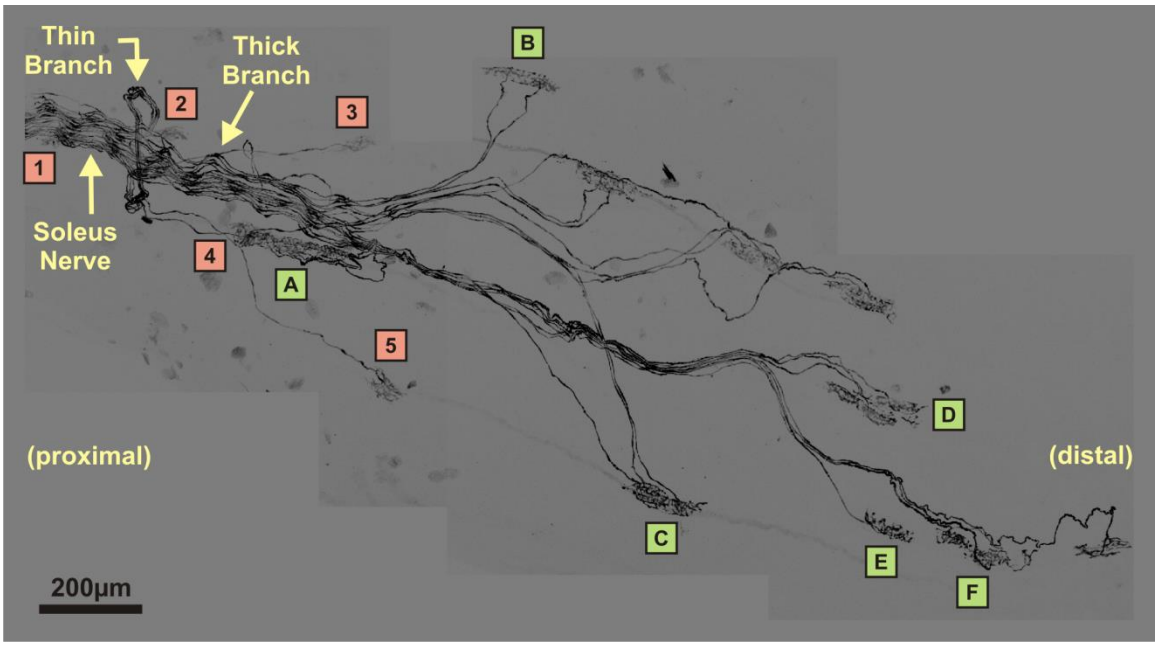
Thin Branch
Thick Branch
B
2
3
1
Soleus Nerve
4
A
5
D
(proximal)
(distal)
C
E
F
200µm

Figure 7. Animal 2: composite 60X images of representative MS (green boxes), and GTOs (pink boxes). (A) The complete proprioceptive innervation of the thin branch. Note the absence of MS here. In this case, only GTOs were present on the thin branch. **(B)** Spindle A was supplied by four proprioceptive axons all via the thick branch. **(C)** Spindle B had two proprioceptive axons. **(D)** Spindle C was supplied by three proprioceptive axons. **(E)** Spindle D had three proprioceptive axons. **(F)** Spindle E had just one proprioceptive axon. **(G)** Spindle F was supplied by two proprioceptive axons.

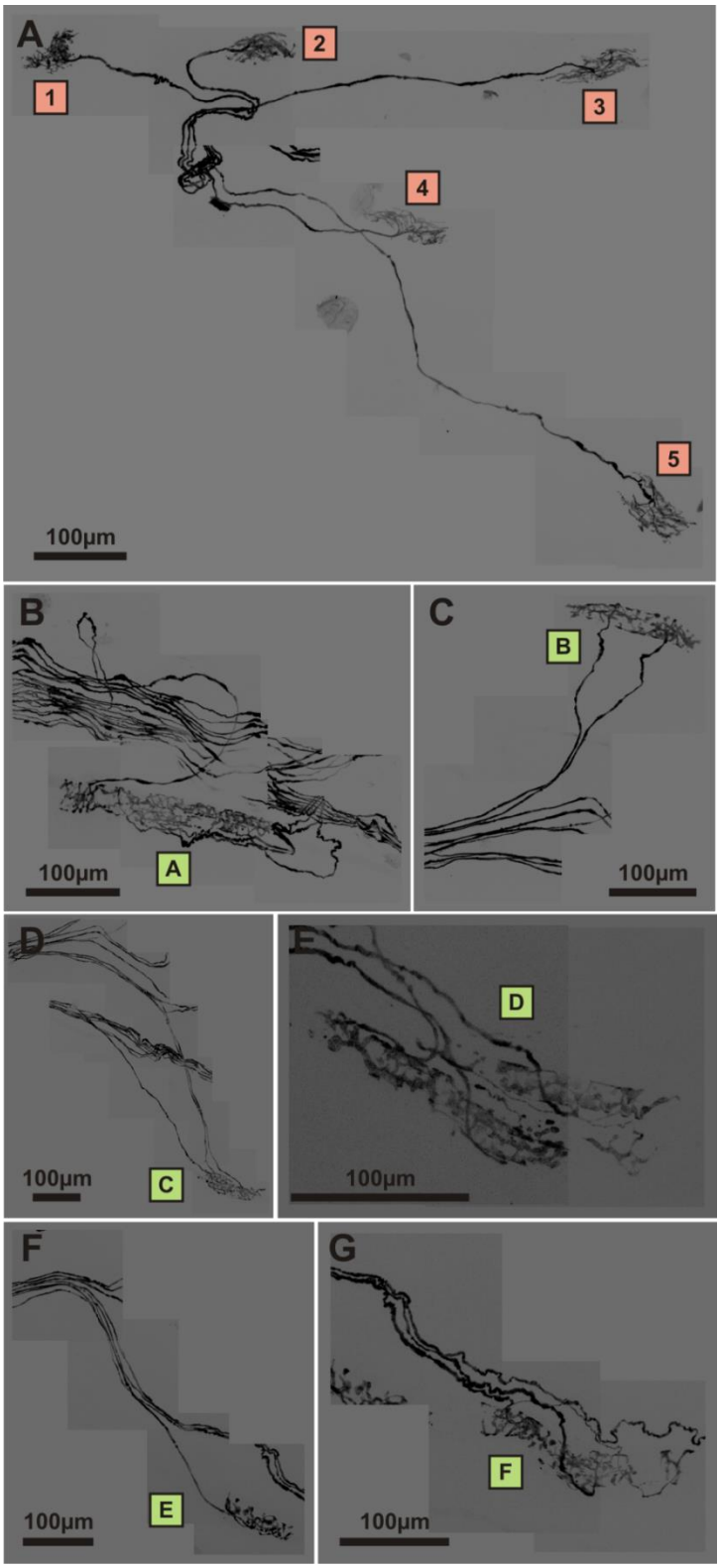
A
1
2
3
4
5
100µm
B
100µm
A
C
B
100µm
D
100µm
C
E
D
100µm
F
100µm
E
G
F
100µm

Figure 8. Animal 3: composite 20X image of proprioceptive innervation within the soleus muscle. Representative MS (green boxes) and GTOs (pink boxes) were selected for high magnification confocal imaging and analysis.

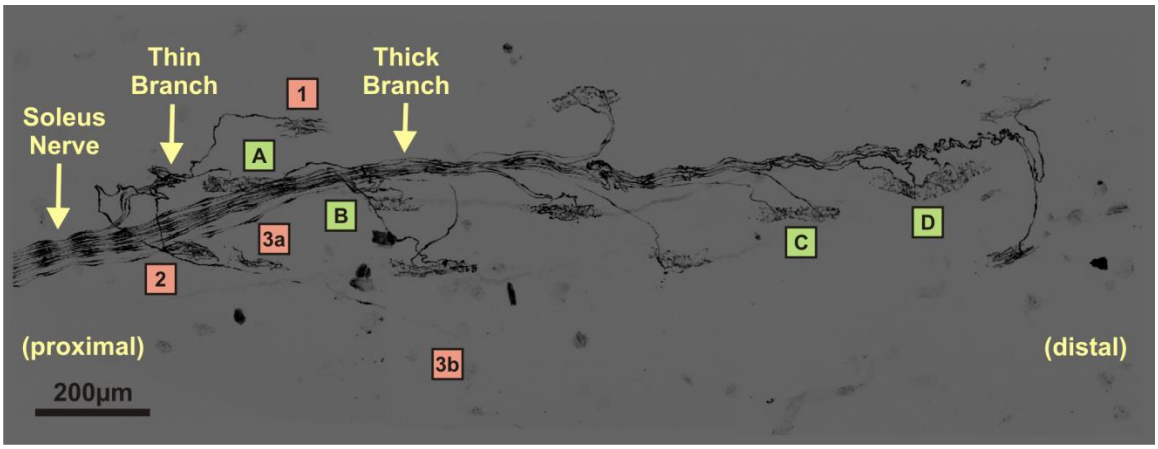
Thin
Branch
Thick
Branch
Soleus
Nerve
1
A
B
3a
2
C
D
(proximal)
3b
(distal)
200µm

Figure 9. Animal 3: composite 60X images of representative MS (green boxes), and GTOs (pink boxes). **(A)** This composite image shows the proprioceptive innervation of this soleus nerve thin branch in its entirety. In this muscle, the thin branch contained four proprioceptive axons, which are all accounted for in this image (three axons to GTOs and one axon to Spindle A). **(B)** Spindle A is supplied by three proprioceptive axons, one via the thin branch and two via the thick branch. Spindle B is an example of a MS supplied by just a single proprioceptive axon. **(C)** Spindle C is an example of a MS supplied by two proprioceptive axons. **(D)** Spindle D is an example of a MS supplied by three proprioceptive axons.

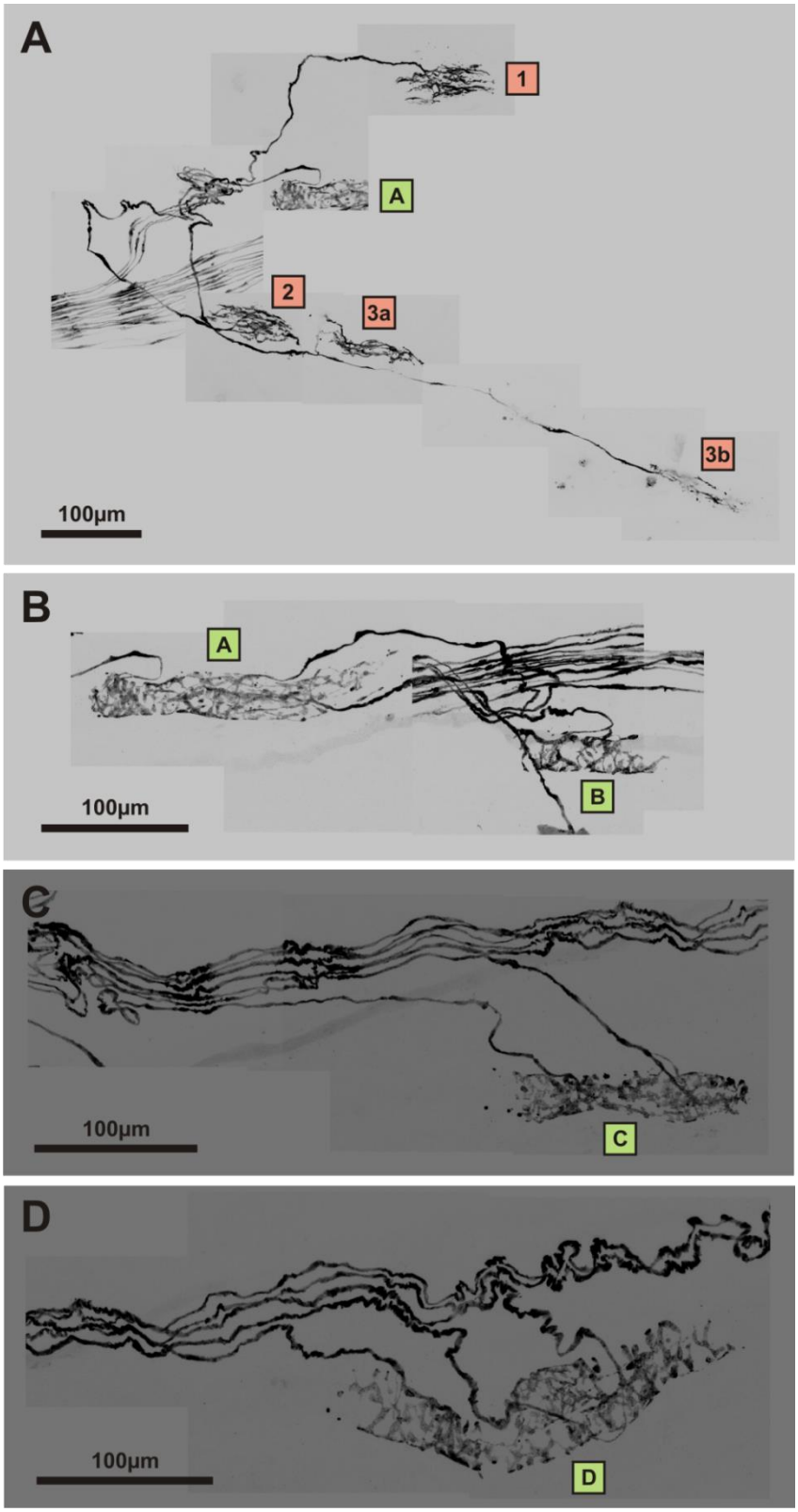
A
1
A
2
3a
3b
100µm
B
A
B
100µm
C
100µm
C
D
100µm
D

Figure 10. Animal 4: composite 20X image of proprioceptive innervation within the soleus muscle. This muscle was unique in that it presented with two thin branches, both with proprioceptive axons supplying MS and GTOs. Compared to the other three muscles, this muscle did have the largest number of proprioceptive axons; however, it did not have the most MS and GTOs. Representative MS (green boxes) and GTOs (pink boxes) were selected for high magnification confocal imaging and analysis.

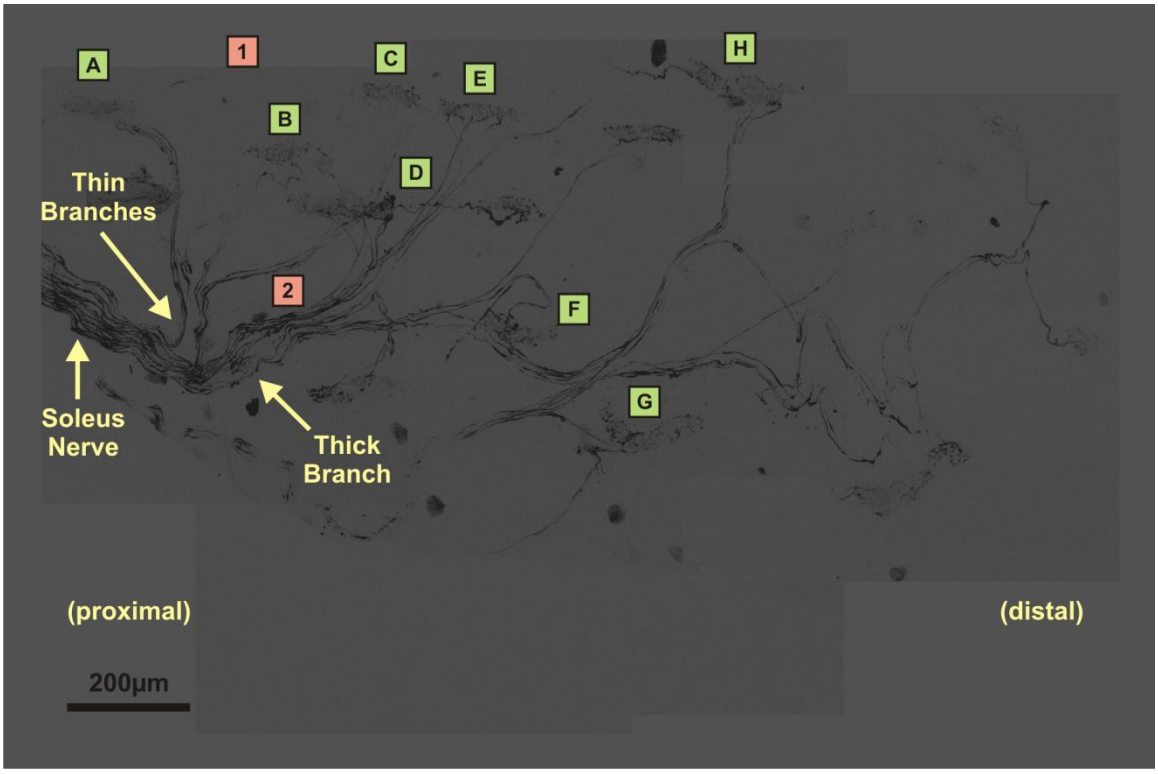
A
1
C
E
H
B
D
Thin
Branches
2
F
G
Soleus
Nerve
Thick
Branch
(proximal)
(distal)
200µm

Figure 11. Animal 4: composite 60X images of representative MS (green boxes), and GTOs (pink boxes). (A) GTO 1 from the more proximal thin branch of the soleus nerve. **(B)** GTO 2 from the more distal thin branch of the soleus nerve. **(C)** Spindle A had three proprioceptive axons all supplied via the proximal thin branch of the soleus nerve. **(D)** Spindles B and C were each supplied two proprioceptive axons, all of which were bundled together with the axon for GTO 2 in the distal thin branch of the soleus nerve. **(E)** Spindle D is the only MS observed in these experiments that was supplied by five proprioceptive axons. **(F)** Spindle E was supplied by two proprioceptive axons; however, each of those axons displayed some branching patterns prior to reaching their termination points at the spindle. **(G)** Spindle F was supplied by two proprioceptive axons. **(H)** Spindle G was supplied by four proprioceptive axons. **(I)** Spindle H was supplied by four proprioceptive axons. Three of those axons were from a common axon bundle that defasciculated together off of the thick branch. The remaining axon came from a different axon bundle that originated from a more proximal defasciculation point on the thick branch.

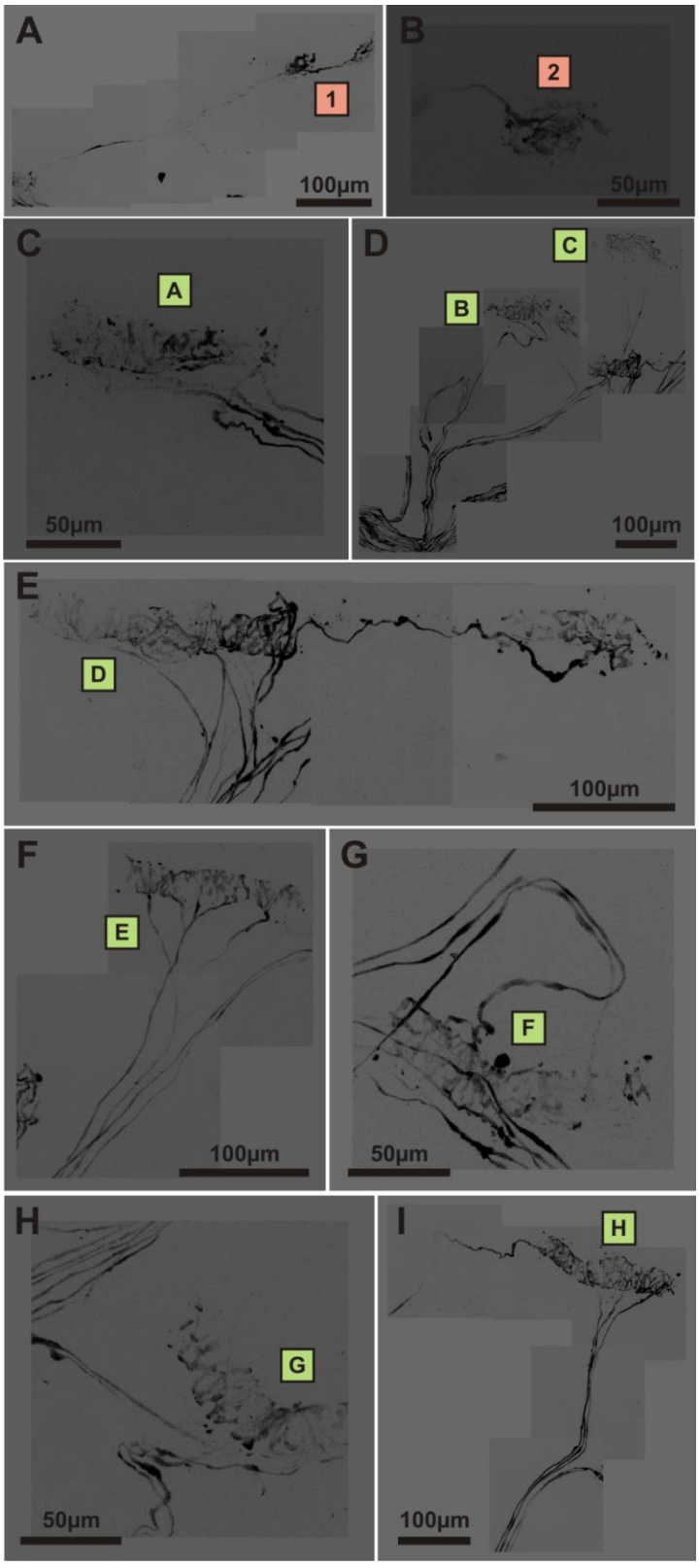
A
1
100µm
B
2
50µm
C
A
50µm
D
C
B
100µm
E
D
100µm
F
E
100µm
G
F
50µm
H
G
50µm
I
H
100µm

Results from confocal imaging confirmed that individual GTOs were consistently innervated by a single proprioceptive axon, namely a Ib afferent (n = 20 GTOs). On the contrary, numbers of proprioceptive axons innervating individual MS were more variable, ranging from 1 to 5 axons. MS innervated by more than one axon (82.1%) were supplied by a combination of Group Ia and II axons. Most frequently, we found a given MS to be supplied by two proprioceptive axons (2.3 ± 0.2, n = 39 spindles, Figure 12). In addition to proprioceptive axon quantification for individual MS and GTOs, the confocal images also allowed us to document the total number of proprioceptive axons housed within the thin branch as well as the whole soleus nerve (Figure 13). In these experiments, we found the soleus nerve to contain proprioceptive axons ranging from 21 to 36 (27.5 ± 3.1) in total. Our analysis further revealed 4 to 9 (6.0 ± 1.1) proprioceptive axons within the thin branch. In all cases, Ib axons were present in the thin branch of the soleus nerve. Spindle afferents, however, were variably present in the thin branch, in populations ranging from 0 to 7 (3.0 ± 1.6).

Overall, the results documented throughout the second aim of this project enabled us to deepen our understanding of the quantities of spindle afferents that innervate the soleus muscle and the possible routes they follow to reach their targets during development. Our analysis suggests that the thin branch of the mouse soleus nerve often contains a mix of Ia and II spindle afferents; however, it occasionally contains muscle spindle afferents of only one type (Figure 7A). As a

Figure 12. Variable numbers of proprioceptive sensory neurons supplied MS within the mouse soleus muscle. Of the 39 total MS analyzed from four different animals, nearly half were supplied by two proprioceptive afferents. Error bars represent ± SEM.

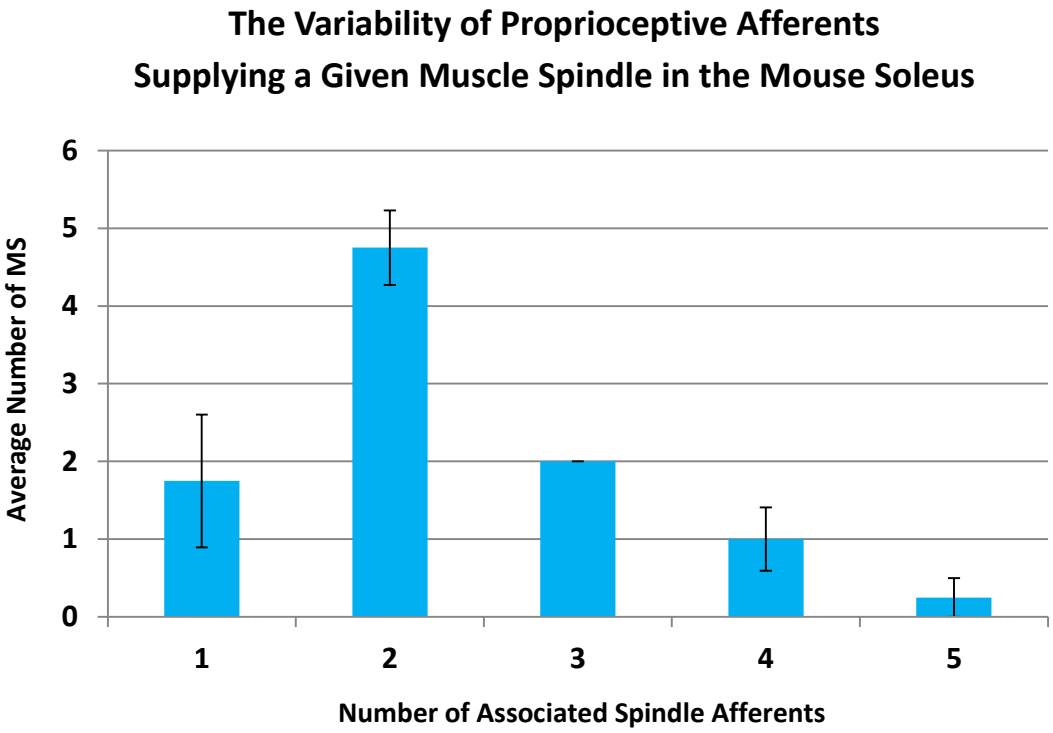
The Variability of Proprioceptive Afferents
Supplying a Given Muscle Spindle in the Mouse Soleus
Average Number of MS
0
1
2
3
4
5
6
1
2
3
4
5
Number of Associated Spindle Afferents

Figure 13. Quantification of proprioceptive axons from cross-sectional views of the thick and thin branches of the soleus nerve agreed with results obtained from the high magnification analysis of MS and GTOs. (A and D) Confocal images (60X) of the proprioceptive axons contained within the soleus thick and thin branches, respectively (Animal 2, PV-Cre/+; Rosa-tdT/+, P5). The yellow dashed line in **(D)** indicates the region of interest shown in **(E)**. **(B and C)** By examining the cross section of this thick branch, we were able to count the 22 proprioceptive axons contained therein, which was equal to the total number of proprioceptive afferents found to supply the MS and GTOs associated with this branch. Vertical yellow line indicates location of cross section. **(E and F)** This thin branch was found to contain five proprioceptive axons, which, interestingly, was also equal to the five axons supplying solely GTOs in this particular animal. Horizontal yellow line indicates the location of cross section. Scale bars represent 10 μm.

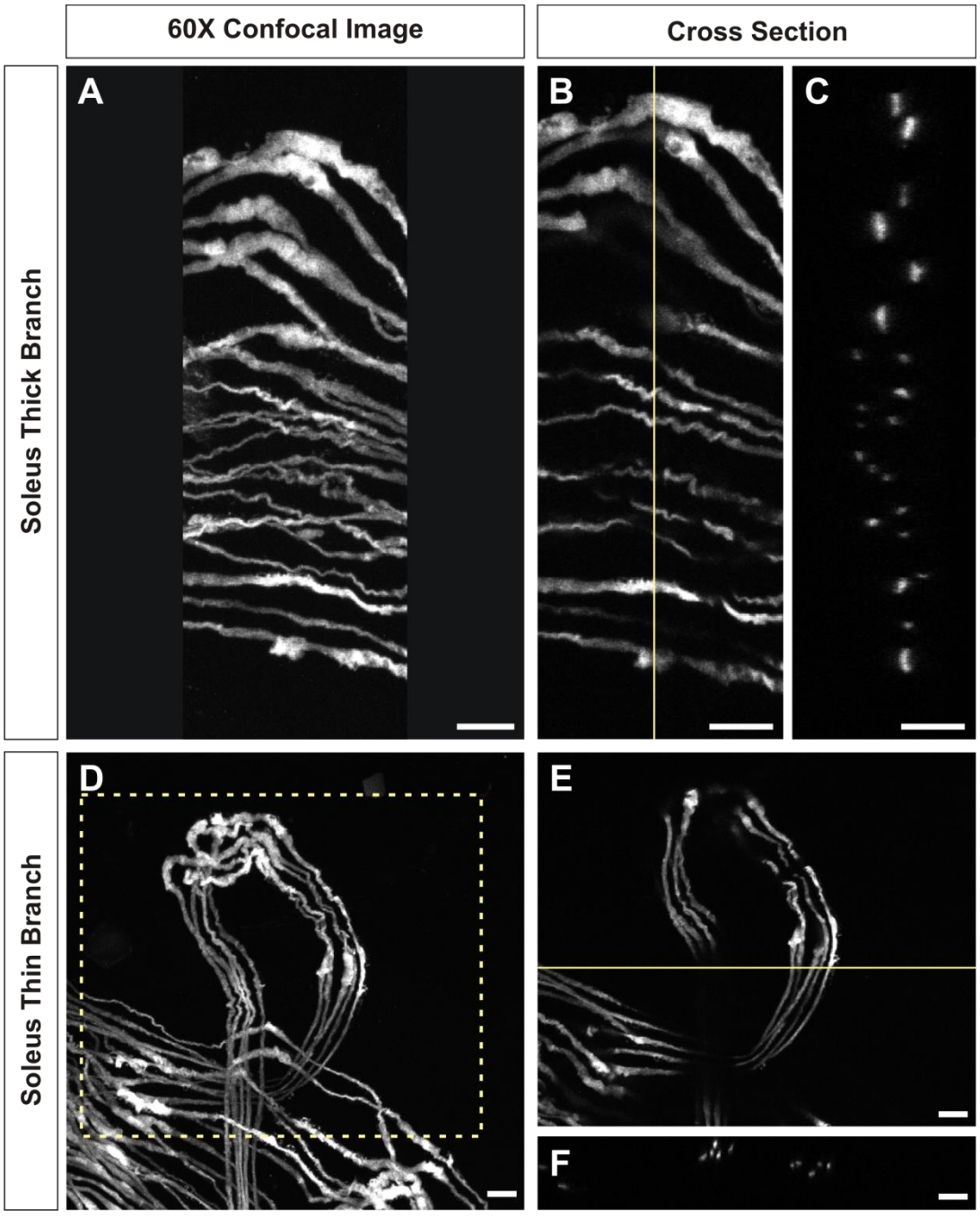
60X Confocal Image
Cross Section
Soleus Thick Branch
Soleus Thin Branch
A
B
C
D
E
F

result, this model system may provide a useful tool in future analysis of muscle spindle and GTO maturation during embryonic and early postnatal development.

Molecular Screening of Proprioceptive Sensory Neurons

The third aim of this project was to collect single fluorescently labeled cells from the DRG and use qRT-PCR to conduct a preliminary screening for differences gene expression among PSNs. We performed retrograde backfills of the quadriceps nerve in 3 WT and 2 PV-Cre/+; Rosa-26/+ animals in order to label a large population of quadriceps-specific sensory neurons in DRG-L3 and DRG-L4. The peripheral nerve supplying the quadriceps muscles, which are responsible for knee extension, was chosen for retrograde tracing due to the large number of proprioceptive afferents contained within it. Previous experiments have demonstrated that filling the quadriceps nerve labels 300 to 400 neurons distributed between the dorsal root ganglia at lumbar segments 3 and 4 (DRG-L3 and DRG-L4, B. Gosky and M. Dallman, personal communication). This approach ensured that a large population of PSNs would be eligible for single cell isolation and molecular screening. In addition, the quadriceps nerve was a logical target for PSN labeling at this stage because future experiments will entail utilizing this nerve for the electrophysiological identification of PSNs via intracellular recordings.

Single cells (n = 13 cells) were then extracted from DRG slices as shown in Figure 14 and subsequently analyzed for expression of 8 genes listed in Table 1. One additional sample served as a negative control and contained solution from a

Figure 14. Illustration of experimental procedure for single-cell capture from DRG slices. This 2-photon image was taken from a P6 WT mouse following peroneal nerve backfill with Rhodamine dextran. The dotted line in each panel represents the approximate outline of the glass pipette used for single-cell capture. **(A)** FITC dextran was pre-loaded into the pipette to aid in visualizing the pipette during navigation to the DRG slice. Here, we show a cell shadow that is created by the fluorescence of the FITC dextran. **(B)** A large cell brightly labeled with rhodamine dextran was successfully captured. Notice that the bright cell within the pipet directly corresponds to the cell shadow observed in **(A)**.

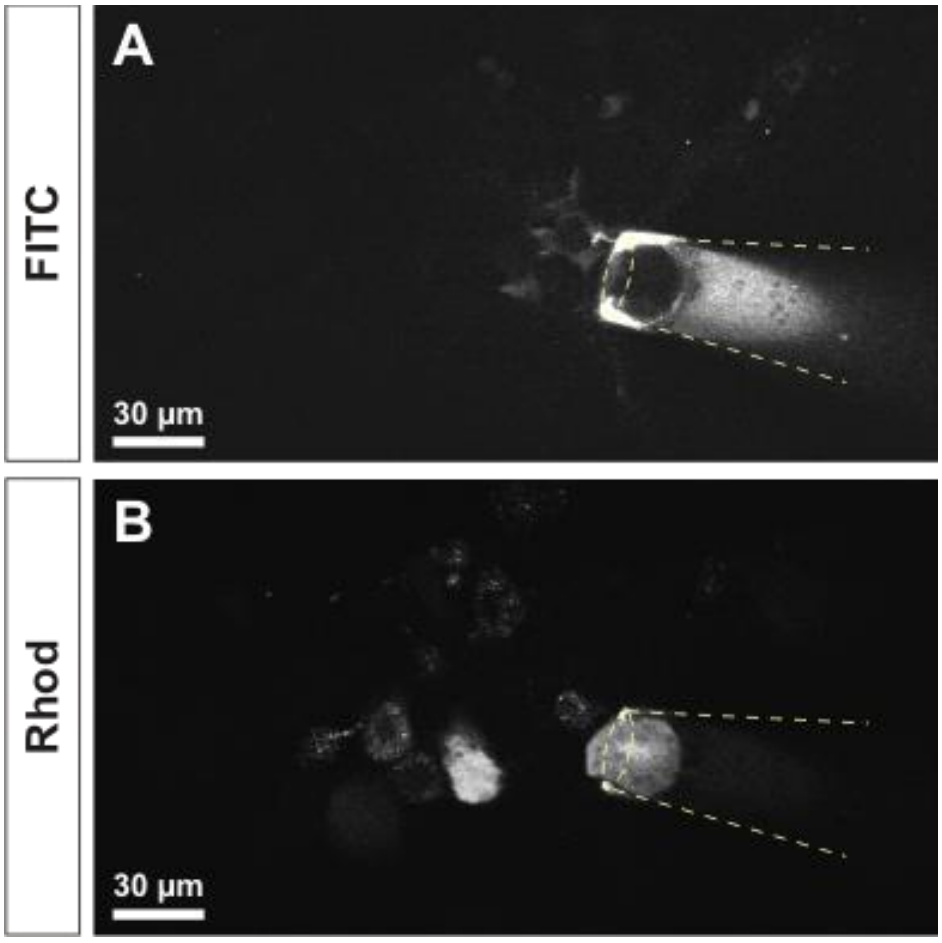
FITC
A
30 µm
Rhod
B
30 µm

pipette in which no cells were aspirated, but that was placed in the chamber near the DRG. No expression of any of the eight genes chosen was detected in this sample. Conversely, all samples containing cellular material showed successful gene expression of the endogenous control gene, *GAPDH*, as illustrated by qRT-PCR amplification data (Figure 15). Furthermore, the well-established marker of DRG neurons, *Isl1*, was detected in all cells (Figure 16). All qRT-PCR reactions were performed in triplicate, which resulted in 336 total wells processed. Of those 336 wells, only 2 were excluded from our results due to inconsistent amplification data. Also, of the 8 genes we selected for screening, *Grm3* was the only target not detected in any of the samples (Figure 19).

In order to compare relative gene expression among PSNs, we first needed to classify each cell as proprioceptive or non-proprioceptive according to the results of gene expression. One cell sample (Cell 12) was specifically chosen as a non-proprioceptive sensory neuron (non-PSN) because of its lack of PV-tdT expression. This served as our calibrator sample when comparing gene expression differences. In these experiments, a cell was classified as a PSN if it co-expressed *Pvalb* and *Runx3* at levels above the non-proprioceptive calibrator sample, Cell 12. Amplification data for *Pvalb* and *Runx3* is presented in Figure 15. Of the 7 WT cells collected, we were only able to identify 1 PSN based on gene expression; however 3 out of the 5 PV-Cre/+; Rosa-tdT/+ cells displayed *Pvalb* and *Runx3* expression at higher levels relative to the calibrator sample (Figure 16). These results imply that, compared to WT, the transgenic mouse model may be the more effective option for

Figure 15. Amplification curves demonstrated technical success of qRT-PCR. All qRT-PCR wells that contained cellular material showed successful gene expression. **(A)** This is the amplification curve for our endogenous control gene, GAPDH. The only sample that did not amplify was our negative control sample that contained only FITC dextran and ACSF (no cellular material). **(B)** Amplification curve for Pvalb shows that all samples amplified except for our negative control sample. **(C)** Amplification curve for Runx3. In addition to the negative control sample, Runx3 was not expressed by Cell 5 and Cell 8. In each graph, Rn represents the normalized reporter signal, which is the emission intensity of the reporter dye divided by the emission intensity of the passive reference dye measured at each cycle.

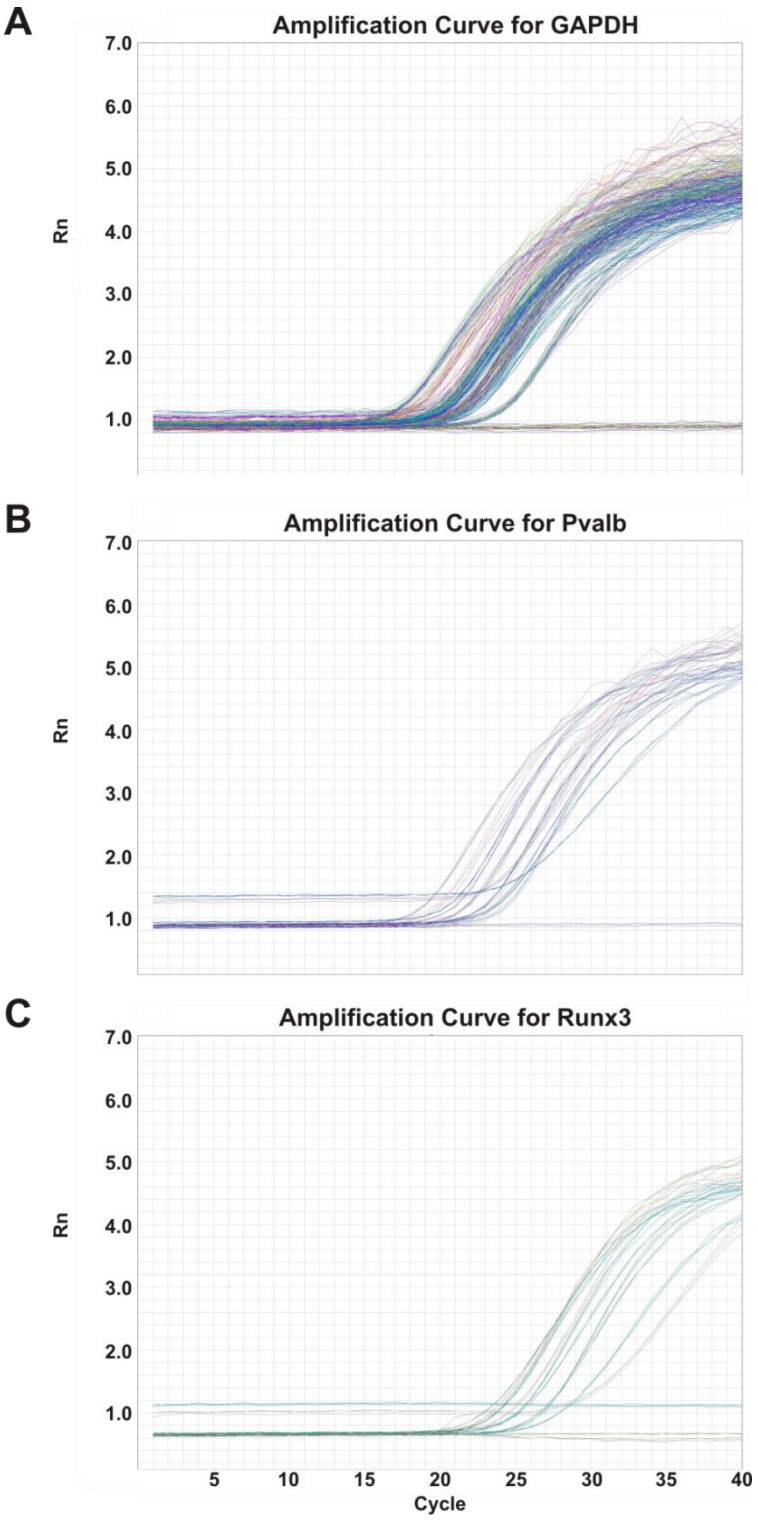
A
Amplification Curve for GAPDH
Rn
7.0
6.0
5.0
4.0
3.0
2.0
1.0
B
Amplification Curve for Pvalb
Rn
7.0
6.0
5.0
4.0
3.0
2.0
1.0
C
Amplification Curve for Runx3
Rn
7.0
6.0
5.0
4.0
3.0
2.0
1.0
5
10
15
20
25
30
35
40
Cycle

Figure 16. Gene expression results for known markers of PSNs. All cells expressed *Isl1*, a well-known marker for DRG neurons. Relative co-expression of *Pvalb* and *Runx3* higher than the non-proprioceptive calibrator sample (Cell 12) was used to confirm PSN identity. As a result, Cell 7 was the only WT cell confirmed to be a PSN. On the other hand, 3 out of the 5 PV-Cre/+; Rosa-tdT/+ cells displayed *Pvalb* and *Runx3* expression at higher levels relative to the calibrator sample. Overall, 4 out of 12 cells collected were confirmed PSNs (highlighted in yellow). Error bars represent 95% confidence interval.

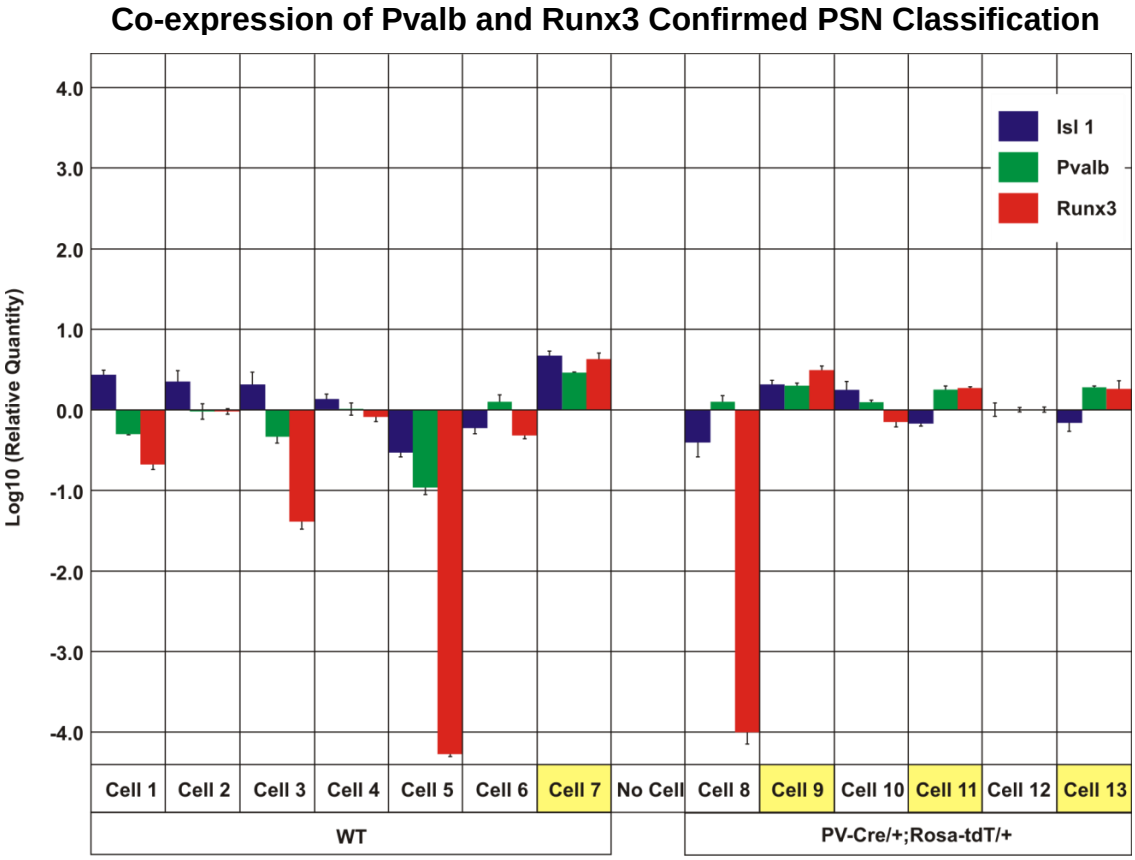
Co-expression of Pvalb and Runx3 Confirmed PSN Classification
Log10 (Relative Quantity)
4.0
3.0
2.0
1.0
0.0
-1.0
-2.0
-3.0
-4.0
Isl 1
Pvalb
Runx3
Cell 1
Cell 2
Cell 3
Cell 4
Cell 5
Cell 6
Cell 7
No Cell
Cell 8
Cell 9
Cell 10
Cell 11
Cell 12
Cell 13
WT
PV-Cre/+;Rosa-tdT/+

isolating PSNs using this technique. Overall, 4 out of 12 cells collected were confirmed PSNs and were thus the focus of the remaining analysis.

When comparing and contrasting the relative expression results of the 4 confirmed PSNs, we made several interesting observations. First, two of the PSNs, Cell 11 and Cell 13, expressed *Gabrg1* at very high levels relative to the calibrator, while the other two did not appear to express it at all (Figure 17). *Gabrg1* encodes the gamma 1 subunit of $GABA_A$ receptors. This data suggests that *Gabrg1* may be expressed by a subset of PSNs. The overall patterns of expression for all tested genes in Cell 11 and Cell 13 were quite similar. Nevertheless, contamination between these samples is unlikely because these two cells were collected from two different animals on separate days. Furthermore, these two cells were also processed for qRT-PCR in two different plates on separate days. Interestingly, two non-PSNs, Cell 1 and Cell 8, also displayed very high levels of *Gabrg1* (Figure 18A). To be clear, the relatively high *Gabrg1* expression levels observed in Cells 1, 7, 8, 11, and 13 are not necessarily indicative of the absolute abundance of the transcript. Inspection of the amplification curve for *Gabrg1* (Figure 18B), demonstrates that when compared to amplification curves of other gene targets, *Gabrg1* required more cycles to reach threshold for detection, and this indicates that *Gabrg1* is a relatively low-copy transcript even in the cells that express it. From these results, we conclude that while *Gabrg1* did not seem to mark a subset of PSNs distinct from all other sensory neurons, *Gabrg1* may be a selective marker of a subset of PSNs.

Figure 17. *Gabrg1* was differentially expressed among confirmed PSNs. Of the four confirmed PSNs, Cell 11 and Cell 13 expressed *Gabrg1* at very high levels relative to the non-proprioceptive calibrator, while Cell 7 and Cell 9 did not express it at all. Error bars represent 95% confidence interval.

Gabrg1 was Differentially Expressed among Confirmed PSNs

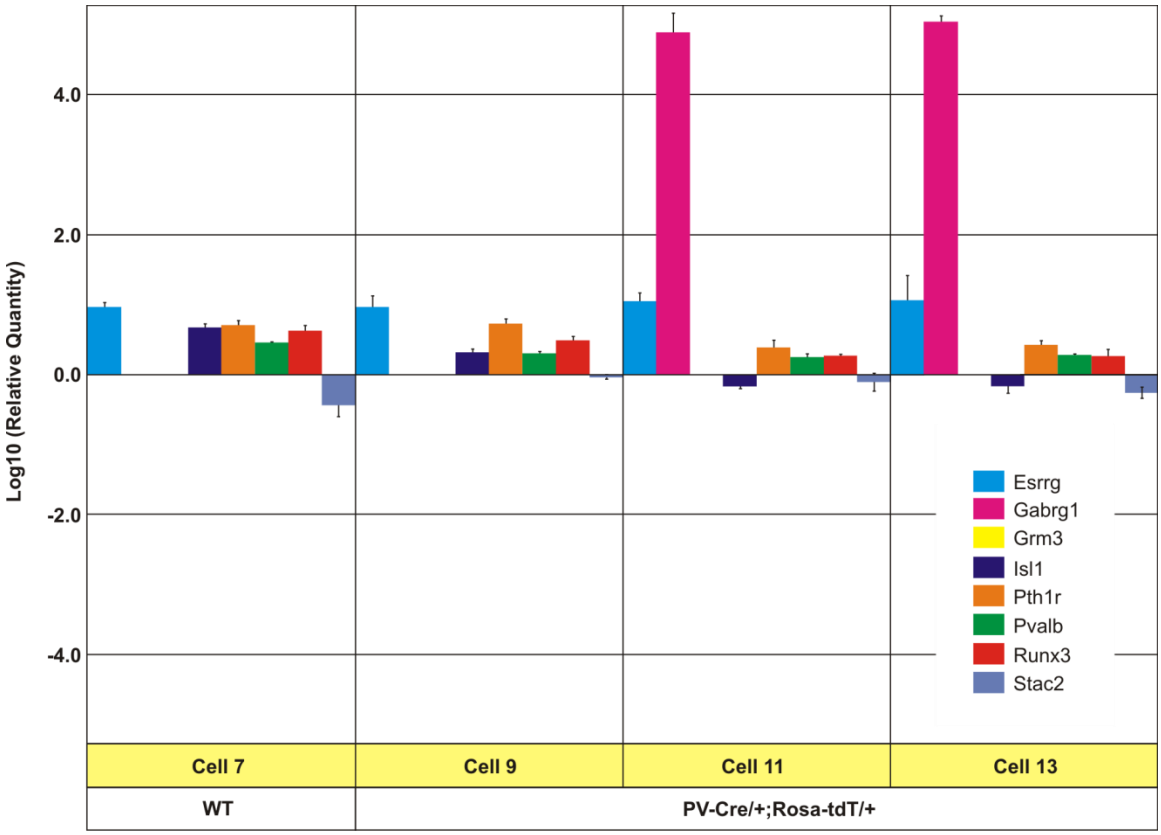

Figure 18. Differential *Gabrg1* expression was not restricted to PSNs. (A) This graph shows the expression of *Gabrg1* in all cells collected. In addition to confirmed PSNs Cell 11 and Cell 13, *Gabrg1* was expressed in two non-PSNs, Cell 1 and Cell 8. PSNs are highlighted in yellow. Error bars represent 95% confidence interval. **(B)** The amplification curve for *Gabrg1* indicates that Cells 1, 8, 11, and 13 did amplify, however, this data suggests that *Gabrg1* transcripts were not abundantly expressed due to the increased number of cycles needed to reach threshold for detection. Cell 12 was the calibrator sample. Rn represents the normalized reporter signal, which is the emission intensity of the reporter dye divided by the emission intensity of the passive reference dye measured at each cycle.

A

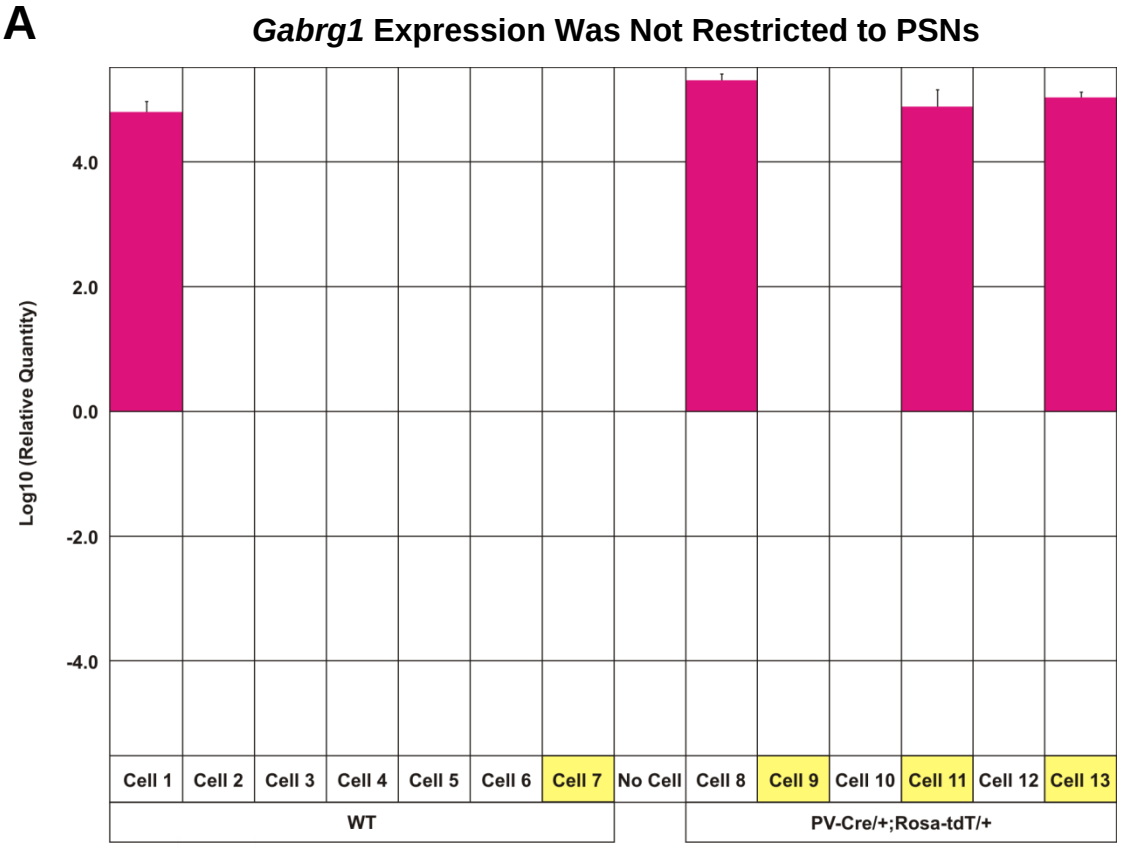
Gabrg1 Expression Was Not Restricted to PSNs
Log10 (Relative Quantity)
4.0
2.0
0.0
-2.0
-4.0
Cell 1
Cell 2
Cell 3
Cell 4
Cell 5
Cell 6
Cell 7
No Cell
Cell 8
Cell 9
Cell 10
Cell 11
Cell 12
Cell 13
WT
PV-Cre/+;Rosa-tdT/+

B

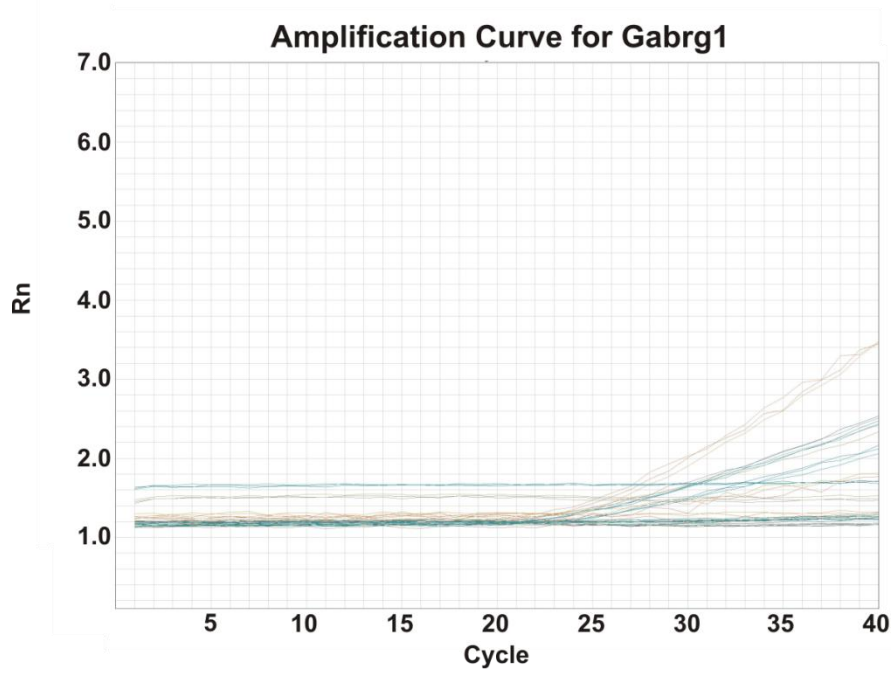
Amplification Curve for Gabrg1
Rn
7.0
6.0
5.0
4.0
3.0
2.0
1.0
5
10
15
20
25
30
35
40
Cycle

Although *Gabrg1* was the only gene to show differential expression in an on-off manner, the results from *Esrrg* (Estrogen-related related receptor gamma) and *Pth1r* (Parathyroid hormone 1 receptor) expression also provided interesting information. *Esrrg* and *Pth1r* were expressed at relatively higher levels in the 4 confirmed PSNs compared to the non-PSNs; therefore, these transcripts could be useful as general markers for PSNs (Figure 19). Finally, *Stac2* (an adapter protein) appeared to be expressed in PSNs at levels similar to that of the calibrator cell, and did not vary in a distinct pattern among cell types in our data set (Figure 19). Taken together, results of Aim 3 establish *Gabrg1* as a candidate for potential genetic differences among PSNs, and Esrrg and Pth1r may be additional markers that define PSNs as a group.

Figure 19. Gene expression results support *Esrrg* and *Pth1r* as positive markers of PSNs. *Esrrg* and *Pth1r* were expressed at higher levels in the four confirmed PSNs compared to the non-PSNs (PSNs highlighted in yellow). *Stac2* appeared to be expressed at relatively lower levels as well as to vary among all cell types**.** *Grm3* was the only gene not detected in any of the samples. Cell 12 was the calibrator sample. Error bars represent 95% confidence interval.

Esrrg and *Pth1r* May Selectively Mark PSNs as a Group

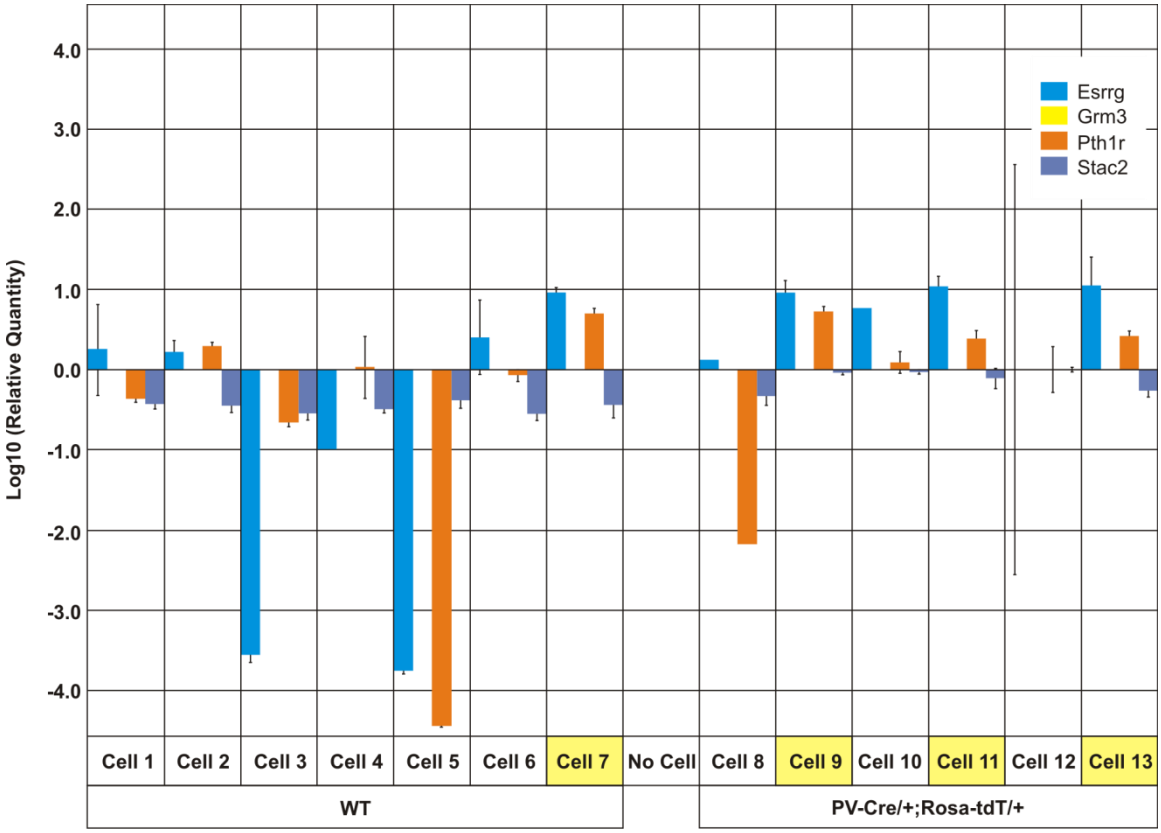

IV. DISCUSSION

For decades, MS and GTOs were commonly observed by preparing ultra-thin transverse or longitudinal serial sections of skeletal muscle for imaging via electron microscopy, and countless micrographs were then reconstructed for analysis (Milburn, 1973; Kozeka and Ontell, 1981; Kucera et al., 1988; Jami, 1992; Zelena, 1996). In addition, a silver staining protocol was applied to teased MS preparations to observe intact structures with light microscopy (Barker and Ip, 1963). Altogether, a wealth of insight and knowledge was gained surrounding the fine ultrastructure and development of MS and GTOs, with MS receiving the majority of investigators' attention. These landmark, but tremendously time consuming, anatomical studies were conducted primarily in cats and rats, although mice are quickly becoming a prevalent model because of the elegant genetic manipulations that are possible (Lionikas et al., 2013).

For this project, we were interested in assessing a transgenic mouse model for the molecular comparison of PSNs that extend their afferent axons specifically to MS or GTOs. The PV-Cre/+; Rosa-tdT/+ mice expressed tdTomato, a dimeric red fluorescent protein in all PSNs, which allowed us to begin by quantifying the entire proprioceptive sensory innervation within the intact soleus muscle. This approach is advantageous because it promises to be much easier to use whole-mount muscle

preparations compared to transverse, thin sections. In Aim 1 of this project, we documented an average of 10.8 ± 0.3 MS in the mouse soleus muscle. The results of these experiments are in good standing with other published results: 12.5 ± 0.5 MS in mice of a BL/6-129SvJ hybrid background (Tourtellotte et al., 2001); 11.2 MS in mice bred on 129/Bl6 and C57Bl/6 backgrounds (Patel et al., 2003); 10 and 11 MS in C57BL/6J mice (Lionikas et al., 2013). In addition, our MS and GTO counts in the thin branch replicated the 1.8 ± 0.4 MS and 2.8 ± 0.2 GTOs reported from serial sections (Tourtellotte et al., 2001). Our optimized whole-mount soleus muscle experiments in PV-Cre/tdT; Rosa-tdT/+ mice allowed not only for rapid quantification of proprioceptive receptors, but also yielded equally informative results compared with other techniques.

The Soleus Muscle: Advantages and Challenges

We selected the soleus as the muscle of interest for the first two aims of this project for three reasons. First, early on in the characterization of the PV-Cre/+; Rosa-tdT/+ mouse model, it became readily apparent that parvalbumin expression was not solely limited to proprioceptive afferents and their endings in the muscle. In fact, at P0 we observed native fluorescence in some extrafusal muscle fibers of certain muscles such as the gluteus maximus and the rectus femoris. By P7, nearly all muscle fibers were brightly labeled making it impossible to discern proprioceptive innervation within skeletal muscle. Mouse skeletal muscles, especially fast muscle fibers, are known to contain high concentrations of

parvalbumin compared to other mammalian species (Heizmann et al., 1982). In the genetic background used in these experiments, however, the C57BL/6J soleus contains predominantly slow muscle fibers (Augusto et al, 2004). We chose to pursue our experiments in the soleus of PV-Cre/+; Rosa-tdT/+ animals and restricted our experimental ages to P3 to P7 in order to avoid the caveat stemming from parvalbumin expression in the muscle fibers. We did explore an alternative approach using Advillin-Cre (Adv-Cre) mice in place of the PV-Cre driver. In these mice, all peripheral sensory neurons are labeled by the fluorescent reporter (Zurborg et al., 2011). When we attempted proprioceptive receptor counts in the soleus muscles of these animals, data collection was hampered by the increased presence of labeled afferents in the muscle. Proprioceptive afferents and receptors were often occluded by presumably Group III and IV muscle afferents to such a degree that definitive MS and GTO counts and axon associations could not be made (data not shown). In order to expand future experiments to other muscles or later developmental stages, it will be necessary to investigate alternate lines of fluorescent reporter mice for a neuronal specific promoter, for instance, that could be more effectively paired with PV-Cre or Adv-Cre driver mice.

A second technical difficulty minimized by the soleus was the confounding factor of light scatter when attempting to image deep into muscle tissue. Compressing the soleus down to a thickness of approximately 200 μm was a critical step in obtaining high quality confocal images for data collection (Vult von Steyern, 1999). Prior to deciding on the compressed muscle preparation, we did attempt

several tissue clearing protocols on uncompressed muscle tissue including tetrahydrofuran (THF) with benzyl alcohol and benzyl benzoate (BABB), Sca*l*e, ethanol and glycerol, and CLARITY (Erturk et al., 2012; Hama et al., 2011; Oliveira, 2010; Chung et al., 2013). The THF and BABB tissue clearing protocol completely quenched the native fluorescence of the PV-Cre/+; Rosa-tdT/+ animals as well as resulted in significant shrinking of the muscle preparation. The remaining clearing protocols we attempted were unsuccessful in rendering muscle tissue optically transparent.

A third reason for choosing the soleus for our experiments was a unique anatomical feature in which the soleus nerve bifurcates into stereotyped thin and thick branches prior to muscle entry (Figure 2). The thin branch of the soleus nerve innervates the proximal compartment of the muscle while the thick branch supplies the remainder of the muscle. Interestingly, a series of retrograde tracing experiments was used to determine that the thin branch does not contain any alpha motor axons; however, it may contain gamma motor axons associated with MS (Vult von Steyern et al., 1999). In our Aim 2 experiments, we found the thin branch of the soleus to contain 4 to 9 (6.0 ± 1.1) proprioceptive axons, which translates to 4 to 9 PSNs housed within DRGs L5 and/or L6. Based on these results, we hypothesized that the thin branch of the soleus nerve could prove to be quite useful in identifying a small subset of PSNs for gene expression analysis via retrograde tracing.

Cell Capture Technique was Optimized Using the Peroneal Nerve

Our Aim 2 results predict that a retrograde backfill of FITC dextran via the soleus nerve thin branch of a PV-Cre/+; Rosa-tdT/+ mouse would result in approximately 4 to 9 PSNs being fluorescently co-labeled between DRG-L5 and DRG-L6. If, for example, we could then enzymatically and mechanically dissociate the DRGs and recover that entire population of co-labeled PSNs for genetic screening, we could look for emergent differences and/or patterns in gene expression among that known population of PSNs (Jankowski et al., 2006). Additionally, having the ability to observe and count the actual MS and GTOs in the intact soleus, as in Aim 1 of this project, we would also be able to know the termination points of all of the thin branch proprioceptive afferents, which could potentially correlate with the gene expression data. Retrograde fills via the whole soleus nerve proved to be technically challenging, however, and filling the thin branch of the soleus nerve was not even attempted at this stage. Technical challenges were further encountered in our efforts with DRG dissociation in that our labeled cell recovery rates were very low (data not shown).

It became clear to us that perhaps having larger populations of labeled DRG neurons available would be advantageous at this stage, as the primary purpose of this thesis is optimizing techniques that would ultimately allow us to make molecular comparisons between PSNs. To this end, we ventured away from the soleus muscle for gene expression analysis; however, the knowledge gained throughout the anatomical characterization of proprioceptive receptors and

afferents in the whole-mount soleus preparation may prove to be invaluable at future stages for the testing of candidate markers of PSN subclasses. We thus opted to perform retrograde backfills with FITC dextran using the peroneal nerve. The peroneal nerve innervates the anterior compartment of the distal hind limb, and sensory neurons sending axons through this nerve are found in DRG-L4 and DRG-L5. By selecting this larger nerve for backfill, we effectively increased the number of labeled cells available for capture. This nerve was used in a pilot experiment conducted as outlined in the methods for Aim 3 using a P4 PV-Cre/+; Rosa-tdT/+ animal. A total of 4 single cells were captured for qRT-PCR: 1 PV-Cre/+; Rosa-tdT cell, 1 FITC dextran labeled cell, and 2 cells that were co-labeled with the tdTomato reporter and FITC dextran. Using qRT-PCR, these cells were screened for the expression of known markers of DRG neurons and PSNs including Islet1 (*Isl1*), parvalbumin (*Pvalb*), and *Runx3* as proof of principle for the cell capture technique (Copray et al., 1994; Ernfors et al., 1994; Honda, 1995; Chen, et al., 2003; Patel et al., 2003; Hippenmeyer et al., 2005; Sun et al., 2008; de Nooij et al., 2013). Results of this pilot experiment were quite encouraging (data not shown), but we chose to focus on backfills of the quadriceps nerve for the remaining experiments in this thesis, as it will directly pertain to future electrophysiological experiments that will take place beyond the scope of this thesis.

tdTomato Crosstalk Obstructed Determination of Muscle-Specific Gene Expression

There is growing evidence that genes common to all PSNs are not uniformly expressed and regulated across PSNs innervating different muscle targets. For example, Er81 is a transcription factor expressed by all PSN, but in $Er81^{-/-}$ animals MS afferents are differentially affected along the proximal/distal axis of the hind limb. Proximal hind limb muscles of $Er81^{-/-}$ animals showed a significant loss of spindle sensory endings, but moving more distally along the hind limb, the loss of spindle sensory endings waned (de Nooij et al., 2013). In fact, in the gastrocnemius and soleus muscles, loss of Er81 actually resulted in an increase in the total number of MS per muscle (Kucera et al., 2002; de Nooij et al., 2013). This sensitivity to loss of Er81 appears to inversely correlate with the amount of NT3 present at peripheral targets. In other words, more distal muscle targets are enriched with NT3 and show lower dependence on Er81 for the differentiation and provision of spindle sensory endings (de Nooij et al., 2013).

With this knowledge in mind, we reasoned it would be important for molecular comparisons to be performed among a subset of PSNs specific to one muscle group, and we settled on the quadriceps. For the WT single cell capture experiments, we retrogradely filled the quadriceps nerve with rhodamine dextran. All of the red labeled cells in DRG-L3 and DRG-L4 represented quadriceps-specific sensory neurons, but may or may not be PSNs. It was therefore imperative to confirm proprioceptive identity according to the co-expression of *Pvalb* and *Runx3*. Of all the WT neurons collected, Cell 7 was the only one that was a confirmed

quadriceps-specific PSN. Analysis of the nerve branch common to the lateral gastrocnemius and soleus muscles in the cat described the sensory fiber composition to be approximately one-third myelinated fibers and two-thirds unmyelinated fibers (Mense, 2010). Not all muscle nerves echo this exact distribution of sensory afferents, however, the presence of unmyelinated muscle afferents in muscle nerves could reasonably contribute to our outcome of only 1 PSN out of 7 WT DRG neurons collected (Mense, 2010; Stacey, 1969).

For the PV-Cre/+; Rosa-tdT/+ single cell capture experiments, all PSNs were genetically labeled red, so we retrogradely filled the quadriceps nerve with FITC dextran in order to secure a quadriceps-specific population of red and green co-labeled PSNs for molecular comparison. It was discovered during the course of these experiments that the intense tdTomato fluorescence actually bleeds through into the FITC channel. In other words, all of the red labeled cells were also visible in the FITC channel, making it very difficult to identify authentic co-labeled PSNs. As a result, we can confidently report that the cells collected from these experiments were PV positive based on red fluorescence; however, these cells may or may not be quadriceps-specific due to the tdTomato crosstalk.

This possibility, in fact, may be demonstrated in our results. In Figure 17, PV-Cre/+; Rosa-tdT/+ Cell 8 and Cell 10 both expressed *Pvalb*, but they were excluded from the PSNs based on relatively low Runx3 expression. Due to the crosstalk factor, it is possible that these cells were not quadriceps-specific, and could rather be representatives of a population of cutaneous mechanoreceptors, including

Pacinian, Meissner, and Lanceolate endings, which are known to express *Pvalb*, but not *Runx3* (de Nooij et al., 2013). To avoid this concern in the future, perhaps using a blue fluorescent dextran (i.e., cascade blue) for retrograde fills or exploring new fluorescent reporter mouse lines would eliminate the crosstalk. It may also be to our advantage to include additional positive marker genes, such as *TrkC* and *Er81* for thorough identification of PSNs.

Rationale for Candidate Gene Targets in Relation to Results from Gene Expression

When compiling a panel of genes to be included in the qRT-PCR screening, we included known markers as well as candidates for differential expression identified in the literature (Table 1). First, Isl1 is a transcription factor common among all DRG sensory neurons, and as expected, all of our captured cells expressed *Isl1* (Sun et al., 2008). *Pvalb*, the gene that encodes the calcium binding protein parvalbumin, has been discussed throughout this thesis as a well-known marker for PSNs (Copray et al., 1994; Ernfors et al., 1994; Honda, 1995; Patel et al., 2003). The transcription factor *Runx3* regulates PSN axonal trajectory to central and peripheral targets and is also known to mark PSNs, especially when *Pvalb* is also expressed (Inoue et al., 2002; de Nooij et al., 2013). Taken together *Isl1*, *Pvalb*, and *Runx3* served as positive controls for the genetic screening and allowed us to confirm the identities of 4 PSNs from our data set.

We hypothesized that the cell fates of PSNs as Group Ia, Ib, and II afferents are genetically pre-programmed. Consequently, we searched the literature for

instances where a particular gene was expressed in a subset of PSNs. While this could represent an incidental finding to others, it could be invaluable in our endeavor to uncover distinct genes expressed by PSN subclasses. In a study by Legha et al., investigators employed Affymetrix microarrays to compare gene expression between WT and $trkA^{trkC/trkC}$ knock-in mice. Inserting *trkC* at the *trkA* locus eliminates the trkA neuronal phenotype and greatly increases the number of neurons having a PSN phenotype in DRG-L5 (Moqrich et al., 2004). Comparing genomic profiles of these mice to WT mice showed that most, but not all TrkC-positive DRG neurons co-expressed stac2, which is an adapter protein likely involved in setting up protein interactions within signaling pathways (Legha et al., 2010; Suzuki et al., 1996). The relative expression from our qRT-PCR results showed that *stac2* varied among all cells collected, and there are a couple of insights that may support this. First, we have a very small sample size represented in our dataset; therefore, differential expression of *stac2* may not have been observed among PSNs. Second, the expression pattern of stac2 in DRG neurons has been shown to change throughout the first postnatal week. At birth, stac2 is restricted to large diameter neurons; however, at some point during the first week of life, this expression spreads to other classes of sensory neurons before finally settling in TrkB and TrkC populations (Legha et al., 2010). Due to this complicated timeline surrounding expression of this gene, we conclude that *stac2* may not be the ideal candidate for detecting class differences among PSNs.

Other putative PSN marker genes, *Esrrg*, *Pth1r*, *Grm3*, and *Gabrg1*, were all gathered from a study that sought to track the effects on gene transcription by varying the amount of NT3 that was available in the periphery (Lee et al., 2012). To begin, the authors used $TrkC^{GFP}$ labeling as a delineator to sort PSNs and non-PSNs. This allowed them to compare and contrast global gene expression between the two groups using Affymetrix gene chip technology. As a result, they were able to identify and confirm many new genes highly expressed in PSNs alone, including *Esrrg*, *Pth1r*, *Grm3*, and *Gabrg1*.

Interestingly, *Esrrg*, which encodes Estrogen-related receptor gamma, had been shown previously to be highly expressed in gamma MNs, but not at all in alpha MNs (Friese et al., 2009; Lee et al., 2012). Because of this precedent for selective expression among subsets of neurons belonging to the same class, we opted to include *Esrrg* in our list of candidates. Our results revealed consistently higher levels of *Esrrg* expression in PSNs versus non-PSNs and so confirmed previous findings by Lee et al. *Pth1r* encodes the Parathyroid hormone 1 receptor and is understood to function in skeletal development; however, a role for *Pth1r* has not been established in the proprioceptive feedback system (Wu et al., 2010). *Pth1r* expression was demonstrated at high levels in PSNs and eliminated completely from the DRG in $TrkC^{-/-}$ mutants, a genetic manipulation that causes PSNs to die (Lee et al., 2012). If expression of a particular gene, in this case *Pth1r*, is found in only a fraction of DRG neurons and is totally absent from the DRG in a PSN-specific knock-out, then it is very likely to be a PSN-specific gene. According to this logic, we

incorporated *Pth1r* into our list of targets for molecular comparison. Our gene expression data likewise placed *Pth1r* at higher relative expression levels in PSNs compared to non-PSNs. Taken together, we conclude that *Esrrg* and *Pth1r* may mark the PSN population inclusively, but neither was expressed in a manner that would suggest selectivity among PSN subclasses.

Similar to *Esrrg* and *Pth1r*, the expression of *Grm3*, which encodes Metabotropic glutamate receptor 3, was effectively eliminated in DRGs of TrkC$^{-/-}$ mice, but its native expression pattern in the DRG was much more scarce compared to the expression patterns of *Esrrg* and *Pth1r* (Lee et al., 2012). Based on this observation, the authors concluded that *Grm3* was expressed by a subpopulation of PSN, which prompted us to screen for *Grm3* expression in our experiments. Our results showed no expression of *Grm3* in any of the cells we collected, yet our endogenous control gene, *GAPDH*, was successfully amplified in the wells shared with *Grm3*. One possibility is that the low density expression of *Grm3* in the DRG reported by Lee et al. combined with our small sample size, means we may not have selected PSNs that expressed it.

Differential Expression of Gabrg1 Among PSNs

Gabrg1 encodes the $GABA_A$ receptor gamma 1 subunit. Briefly, $GABA_A$ receptors are pentameric ligand-gated ion channels, containing 2 alpha subunits, 2 beta subunits and 1 gamma subunit, all of which have multiple isoforms (Nicholls et al., 2012). *Gabrg1* was a central focus for Lee et al. because varying the amount of

NT3 produced the most dramatic effects on *Gabrg1* transcription in confirmed PSNs (Lee et al., 2012). In other words, when NT3 was abolished, *Gabrg1* expression was nearly absent in PSNs, and when NT3 was elevated, *Gabrg1* showed increased expression (Lee et al., 2012). *Gabrg1* was also shown to be distributed unevenly in segments along the rostral-caudal axis. Expression was lowest in L1 and increased in caudal segments, peaking in L5. L6 expression, however, was similar to that in L1. This differential expression is in contrast to expression of *TrkC* and *Pvalb*, which remain stable through these segments. Also, this rostral-caudal pattern of *Gabrg1* expression tended to persist into adulthood (Lee et al., 2012). These interesting findings, along with the potential synaptic implications and biological relevance of $GABA_A$ receptors in PSNs, piqued our curiosity and led us to include *Gabrg1* in our single cell qRT-PCR screening.

Perhaps the most striking observation made during this project arose while comparing relative expression of *Gabrg1* among 4 molecularly identified PSNs (Figure 17). In our experiments, Cells 11 and 13 expressed *Gabrg1*, while Cells 7 and 9 did not. This finding suggests the possibility of differential expression of $GABA_A$ receptor subunits among PSNs. Currently, three gamma subunit isoforms have been described and all have been detected in cultured embryonic and adult human DRGs according to mRNA expression (Maddox et al., 2004). It would be worthwhile to include all gamma subunits in future molecular screenings of larger samples of PSNs in order to further test for differential expression of these $GABA_A$ receptor subunits. Variability in $GABA_A$ receptor subunit composition is known to

have important pharmacological and synaptic functions. For example, $GABA_A$ receptors having the gamma 2 subunit are able to bind benzodiazepine drugs (Pritchett et al., 1989). In addition, the gamma 2 subunit was believed to be the predominant subunit capable of clustering $GABA_A$ receptors postsynaptically until one study found that the gamma 3 subunit served as functional substitute in gamma $2^{-/-}$ animals, although with slower kinetics (Kerti-Szigeti et al., 2014). Finally, HEK293 cells transfected with $GABA_A$ receptors composed of alpha 2 and gamma 1 subunits together were reported to yield slower inhibitory post-synaptic current kinetics (Dixon et al., 2014). In PSNs, perhaps this particular subunit composition would enhance primary afferent depolarization, which will be further discussed later in this section.

The functional implication of $GABA_A$ receptors found in PSNs relates to the fine-tuning of sensory feedback through the process of presynaptic inhibition. Presynaptic inhibition of sensory afferents is accomplished via central axo-axonic synapses of a GABAergic interneuronal subpopulation onto the afferent terminals, including Group Ia, Ib, and II (Maxwell and Bannatyne 1983; Alvarez, 1998; Rudomin and Schmidt, 1999; Betley et al., 2009). The transcription factor Ptf1a is a molecular marker for these GABAergic interneurons, termed GABApre neurons, which mediate presynaptic inhibition of primary afferents (Glasgow et al, 2005; Betley et al., 2009). In contrast to other central nervous system neurons, mature primary sensory neurons maintain a high intracellular Cl^- concentration through the work of a Na^+-K^+-$2Cl^-$ cotransporter (Alvarez-Leefmans, 2009). Upon binding the

neurotransmitter gamma-aminobutyric acid (GABA), primary sensory afferents are known to depolarize as a result of Cl^- efflux. This primary afferent depolarization decreases the amount of neurotransmitter release, and is a hallmark of presynaptic inhibition. The exact mechanism underlying primary afferent depolarization remains to be determined, but two hypotheses appear to be prevalent in the literature (Kullmann et al., 2005). First, primary afferent depolarization may cause Na^+ channels to inactivate and the action potential amplitude to decrease. Less Ca^{2+} influx would cause a decline in vesicular release of neurotransmitter (Graham and Redman, 1994). An alternative shunting hypothesis proposes that depolarizing Cl^- efflux through $GABA_A$ receptors located upstream of the afferent neurotransmitter release site disturbs propagation of action potentials and lessens subsequent neurotransmitter exocytosis (Cattaert and El Manira, 1999).

Recently, GABApre neurons were genetically isolated and manipulated based on expression of Gad2, an enzyme involved in the synthesis of GABA (Fink et al., 2014). Optogenetic stimulation of the GABApre neurons evoked primary afferent depolarization as well as inhibited neurotransmitter release as predicted. The presynaptic inhibitory activity of GABApre neuron population limits the amount of sensory feedback that actually reaches the afferent targets including MNs and other interneurons. To examine the behavioral consequences that ensue in the absence of GABApre neurons, Fink et al. genetically incorporated a diphtheria toxin receptor into the Gad2-expressing neurons via viral injection at spinal segments C3 to T1. Immunohistochemical analysis of Gad2 contacts onto VGLUT1 positive afferent

terminals confirmed that delivery of diphtheria toxin almost completely ablated the GABApre neuronal population. As a result, sensory feedback was left unchecked, and these mice lost the ability to execute smooth motions in the forelimb. For example, when the mice performed reaching tasks, oscillations in motor output caused the forelimb to advance and reverse often while attempting the task (Fink et al., 2014). Interestingly, this behavioral phenotype was not observed when the mice were at rest, which implicated PSNs as the source of overwhelming feedback when movements were attempted.

Not long ago, it was also shown that GABApre neurons rely on signals from proprioceptive afferent terminals for synapse formation (Betley et al., 2009). Using an $Er81^{-/-}$ animal model where PSN terminals in the ventral horn are absent, the GABApre neurons failed to form any synaptic connections at all, even with other INs or MNs in the ventral horn, which suggests that the wiring of this circuit is absolute, not preferential. It would be interesting to determine if presynaptic inhibitory circuit assembly is accomplished differently on Group Ia, Ib, and II afferents, perhaps even according to differences in $GABA_A$ receptor subunit expression.

Another perspective to consider in the interpretation of our results revealing differential *Gabrg1* expression among PSNs focuses on the development of presynaptic inhibition. Electrophysiological experiments in early postnatal mice have shown that presynaptic inhibition of Group Ia afferents, evoked by sensory stimulation, was absent at P0, but present at P7 (Sonner and Ladle, 2013). Parallel findings have been reported in the context of the development of primary afferent

axo-axonic contacts by Ptf1a-expressing GABApre neurons (Betley et al., 2009). At P0 to P2, GABApre neurons contacted afferent terminals anatomically, but lacked GAD65 and GAD67, markers of GABAergic synapses. By P7, however, GAD65 and GAD67 were highly expressed, which supports the electrophysiological results from Sonner and Ladle. It is plausible, therefore, that the differences we observed in Gabrg1 expression arose as a function of a normal developmental timeline. For example, all PSNs may ultimately express *Gabrg1*, but upregulation occurs at different developmental time points. It could be interesting to explore potential differences in the maturation of PSN subclasses through the lens of the development of presynaptic inhibition.

Conclusions and Future Directions

This thesis work established a foundation of experimental techniques to be built upon with further investigations into the molecular comparison of PSN subclasses. We hypothesize that PSN subclasses associated with Group Ia, Ib, and II afferents are molecularly distinct to a degree that would lead to biologically relevant genetic manipulations and new avenues to study the role of proprioceptive sensory feedback on motor functions. To date, we have identified one candidate gene, *Gabrg1*, which appears to be expressed in a subset of DRG-L3 and L4 PSNs at ages P4-P5. This exciting result suggests that there could be much to gain in expanding our efforts in studying PSN gene expression. Experimental methods will need to be refined in the future in order to eliminate certain confounding factors and add

strength to the results obtained. In addition, options for performing genome-wide expression studies on single cells are currently limited due to the low quantity of genetic material provided by a single cell. Perhaps pooling captured cells from PSN subclasses defined by physiological criteria would provide sufficient genetic material for higher input gene expression techniques such as gene chip microarrays. Having the ability to study the independent contributions of PSN subclasses during different motor behaviors could have a profound impact on progress made in the fields of sensory-motor development, recovery from injury, and management of disease.

V. BIBLIOGRAPHY

Alvarez, F. J. (1998). Anatomical Basis for Presynaptic Inhibition of Primary Sensory Fibers. In *Presynaptic Inhibition and Neural Control* (pp. 13-49), New York: Oxford University Press.

Alvarez-Leefmans, F., J. (2009). Chloride Transporters in Presynaptic Inhibition, Pain and Neurogenic Inflammation. In *Physiology and Pathology of Chloride Transporters and Channels in the Nervous System* (pp. 440-470), Amsterdam: Elsevier.

Arber, S., Ladle, D. R., Lin, J. H., Frank, E., & Jessell, T. M. (2000). ETS Gene *Er81* Controls the Formation of Functional Connections between Group Ia Sensory Afferents and Motor Neurons. *Cell,* 101, 485-498.

Augusto, V., Padovani, C. R., & Campos, G. E. R. (2004). Skeletal Muscle Fiber Types in C57BL6J Mice. *Brazilian Journal of Morphological Sciences, 21*(2), 89-94.

Banks, R. W. (2005). The Muscle Spindle. In *Peripheral Neuropathy* (4th ed., Vol. 1, pp. 131-150). Philadelphia: Elsevier.

Betley, J. N., Wright, C. V. E., Kawaguchi, Y., Erdélyi, F., Szabó, G., Jessel, T. M., & Kaltschmidt, J., A. (2009). Stringent Specificity in the Construction of a GABAergic Presynaptic Inhibitory Circuit. *Cell, 139,* 161-174.

Bewick, G. S. & Banks, R. W. (2014). Mechanotransduction in the Muscle Spindle. *European Journal of Physiology, Epup ahead of print.*

Boyd, I. A. (1980). The Isolated Mammalian Muscle Spindle. *Trends in Neuroscience, 3,* 258-265.

Boyd, I. A. & Smith, R. S. (1984) The Muscle Spindle. In *Peripheral Neuropathy* (2nd ed., pp. 171-202). London: Saunders.

Brown, A. G. (1981). *Organization in the Spinal Cord: the Anatomy and Physiology of Identified Neurones.* Berlin: Springer-Verlag.

Brown, A. G. & Fyffe, R. E. (1978). The Morphology of Group Ia Afferent Fibre Collaterals in the Spinal Cord of the Cat. *Journal of Physiology, 274,* 111-127.

Brown, A. G. & Fyffe, R. E. (1979). The Morphology of Group Ib Afferent Fibre Collaterals in the Spinal Cord of the Cat. *Journal of Physiology, 296,* 215-228.

Burke, R. E., Strick, P. L., Kanda, K., Kim, C. C., & Walmsley, B. (1977). Anatomy of medial gastrocnemius and soleus motor nuclei in cat spinal cord. *Journal of Neurophysiology, 40*(3), 667-680.

Cattaert, D. & El Manira, A. (1999). Shunting Versus Inactivation: Analysis of Presynaptic Inhibitory Mechanisms in Primary Afferents of the Crayfish. *Journal of Neuroscience, 19*(4), 6079-6089.

Chen, A., de Nooij, J. C., & Jessell, T. M. (2006). Graded Activity of Transcription Factor Runx3 Specifies the Laminar Termination Pattern of Sensory Axons in the Developing Spinal Cord. *Neuron, 49,* 395-408.

Chen, H., Hippenmeyer, S., Arber, S., & Frank, E. (2003). Development of the Monosynaptic Stretch Reflex Circuit. *Current Opinion in Neurobiology, 13,* 96-102.

Chung, K., Wallace, J., Kim, S., Kalyanasundaram, S., Andalman, A. S., Dadidson, T. J., …Deisseroth, K. (2013). Structural and Molecular Interrogation of Intact Biological Systems. *Nature, 497*(7449), 332-337.

Copray , J. C., Mantingh-Otter, I. J., & Brouwer, N. (1994). Expression of calcium-binding proteins in the neurotrophin-3-dependent subpopulation of rat embryonic dorsal root ganglion cells in culture. *Developmental Brain Research, 81*, 57-65.

Dallman, M. A. & Ladle, D. R. (2013). Quantitative Analysis of Locomotor Defects in Neonatal Mice Lacking Proprioceptive Feedback. *Physiology & Behavior, 120,* 97-105.

de Nooij, J. C., Doobar, S., & Jessell, T. M. (2013). Etv1 Inactivation Reveals Proprioceptor Subclasses that Reflect the Level of NT3 Expression in Muscle Targets. *Neuron, 77*, 1055-1068.

Dixon, C., Sah, P., Lynch, J. W., & Keramidas, A. (2014). $GABA_A$ Receptor α and γ Subunits Shape Synaptic Currents via Different Mechanisms. *Journal of Biological Chemistry, 289,* 5399-5411.

Eccles, J. C., Fatt, P., & Landgren, S. (1956). Central Pathway for Direct Inhibitory Action of Impulses in Largest Afferent Nerve Fibres to Muscle. *Journal of Neurophysiology, 19*(1), 75-98.

Eccles, J. C., Fatt, P., Landgren, S., & Winsbury, G. J. (1954). Spinal Cord Potentials Generated by Volleys in the Large Muscle Afferents. *Journal of Physiology, 125,* 590-606.

Eldred, E., Bridgman, C. F., Swett, J. E., & Eldred, B. (1962) Quantitative Comparisons of Muscle Receptors of the Cat Medial Gastrocnemius, Soleus and Extensor Digitorum Brevis Muscles. In: *Symposium on Muscle Receptors* (pp. 207-213). Hong Kong: Hong Kong University Press.

Ernfors, P., Lee, K. F., Kucera, J., & Jaenisch, R. (1994). Lack of Neurotrophin-3 Leads to Deficiencies in the Peripheral Nervous System and Loss of Limb Proprioceptive Afferents. *Cell, 77*, 503-512.

Ertürk, A., Mauch, C. P., Hellal, F., Föstner, F., Keck, T., Becker, K.,…Bradke, F. (2012). Three-Dimensional Imaging of the Unsectioned Adult Spinal Cord to Assess Axon Regeneration and Glial Responses After Injury. *Nature Medicine, 18*(1), 166-172.

Fink, A. J. P., Croce, K., R., Huang, Z. J., Abbott, L. F., Jessell, T. M., & Azim, E. (2014). Presynaptic Inhibition of Spinal Sensory Feedback Ensures Smooth Movement. *Nature, 509,* 43-48.

Friese, A., Kaltschmidt, J. A., Ladle, D. R., Sigrist, M., & Jessell, T. M. (2009). Gamma and Alpha Motor Neurons Distinguished by Expression of Transcription Factor Err3. *Proceedings of the National Academy of Sciences, 106*, 13588-13593.

Glasgow, S. M., Henke, R. M., Macdonald, R. J., Wright, C. V., & Johnson, J. E. (2005). Ptf1a Determines GABAergic over Glutamatergic Neuronal Cell Fate in the Spinal Cord Dorsal Horn. *Development, 132,* 5461-5469.

Graham, B. & Redman, S. (1994). A Simulation of Action Potentials in Synaptic Boutons During Presynaptic Inhibition. *Journal of Neurophysiology, 71*(2), 538-549.

Haftel, V. K., Bichler, E., K., Nichols, T. R., Pinter, M. J., & Cope, T. C. (2004). Movement Reduces the Dynamic Response of Muscle Spindle Afferents and Motoneuron Synaptic Potentials in Rat. *Journal of Neurophysiology, 91,* 2164-2171.

Hama, H., Kurokawa, H., Kawano, H., Ando, R., Shimogori, T., Noda, H.,…Miyawaki, A. (2011). Sca*l*e: a Chemical Approach for Fluorescence Imaging and Reconstruction of Transparent Mouse Brain. *Nature Neuroscience, 14*(11), 1481-1488.

Hasan, Z. & Houk, J. C. (1975). Analysis of Response Properties of Deefferented Mammalian Spindle Receptors Based on Frequency Response. *Journal of Neurophysiology, 38*(3), 663-672.

Heizmann, C. W., Berchtold, M. W., & Rowlerson, A. M. (1982). Correlation of Parvalbumin concentration with Relaxation Speed in Mammalian Muscles. *Proceedings of the National Academy of Sciences, 79*(23), 7243-7247.

Hippenmeyer, S., Vrieseling, E., Sigrist, M., Portmann, T., Laengle, C., Ladle, D. R., & Arber, S. (2005). A Developmental Switch in the Response of DRG Neurons to ETS Transcription Factor Signaling. *PLoS Biology, 3*(5), 878-890.

Honda, C. N. (1995). Differential distribution of calbindin-D28k and parvalbumin in somatic and visceral sensory neurons. *Neuroscience, 68*(3), 883-892.

Honeycutt, C. F., Nardelli, P., Cope, T. C., & Nichols, T. R. (2012). Muscle Spindle Responses to Horizontal Support Surface Perturbation in the Anesthetized Cat: Insights into the Role of Autogenic Feedback in Whole Body Postural Control. *Journal of Neurophysiology, 108,* 1253-1261.

Houk, J., & Henneman, E. (1967). Responses of Golgi Tendon Orgns to Active Contractions of the Soleus Muscle of the Cat. *Journal of Neurophysiology, 30*(3), 466-481.

Houk, J. C., Singer, J. J., & Henneman, E. (1971). Adequate Stimulus for Tendon Organs With Observations on Mechanics of Ankle Joint. *Journal of Neurophysiology, 34*(6), 1051-1065.

Hunt, C. C., & Kuffler, S. W., (1951). Stretch Receptor Discharges During Muscle Contraction. *Journal of Physiology, 113*, 298-315.

Inoue, K., Ozaki, S., Shiga, T., Ito K., Masuda, T., Okado, N.,…Ito, Y. (2002). *Runx3* Controls the Axonal Projection of Proprioceptive Dorsal Root Ganglion Neurons. *Nature Neuroscience, 5*(10), 946-954.

Jami, L. (1992). Golgi Tendon Organs in Mammalian Skeletal Muscle: Functional Properties and Central Actions. *Physiological Reviews, 72*(3), 623-666.

Jankowska, E. (1992). Interneuronal Relay in Spinal Pathways from Proprioceptors. *Progress in Neurobiology, 38,* 335-378.

Jankowski, M. P., Cornuet, P. K., McIlwrath, S. Keorber, H. R., & Albers, K. M. (2006). SRY-Box Containing Gene 11 (Sox11) Transcription Factor is Required for Neuron Survival and Neurite Growth. *Neuroscience*, *143*(2), 501-514.

Jansen, J. K. S. & Matthews, P. B. C. (1962). The Effects of Fusimotor Activity on the Static Responsiveness of Primary and Secondary Endings of Muscle Spindles in the Decerebrate Cat. *Acta Physiologica Scandinavica, 55,* 376-386.

Kerti-Szigeti, K., Nusser, Z. & Eyre, M. D. (2014). Synaptic $GABA_A$ Receptor Clustering without the $\gamma 2$ Subunit. *Journal of Neuroscience, 34*(31), 10219-10233.

Klein, R., Silos-Santiago, I., Smeyne, R. J., Lira, S. A., Brambilla, R., Bryant, S.,…Barbacid, M. (1994). Disruption of the Neurotrophin-3 Receptor Gene *trkC* Eliminates Ia Muscle Afferents and Results in Abnormal Movements. *Nature, 368*(6468), 249-251.

Kozeka, K., & Ontell, M. (1981). The Three-Dimensional Cytoarchitecture of Developing Murine Muscle Spindles. *Developmental Biology, 87,* 133-147.

Kucera, J., Walro, J. M., & Reichler, J. (1988). Innervation of Developing Intrafusal Muscle Fibers in the Rat. *The American Journal of Anatomy, 183,* 344-358.

Kucera, J., Cooney, W., Que, A., Szeder, V., Stancz-Szeder, H., Walro, J. (2002). Formation of Supernumerary Muscle Spindles at the Expense of Golgi Tendon Organs in ER81-deficient Mice. *Developmental Dynamics, 223*(3), 389-401.

Kullmann, D., Ruiz, A., Rusakov, D. M., Scott, R., Semyanov, A., & Walker, M. C. (2012). Presynaptic, Extrasynaptic and Axonal $GABA_A$ Receptors in the CNS: Where and Why? *Progress in Biophysics and Molecular Biology, 87*(1), 33-46.

Lee, J., Friese, A., Mielich, M., Sigrist, M., & Arber, S. (2012). Scaling Proprioceptor Gene Transcription by Retrograde NT3 Signaling. *PLoS One, 7*(9), e45551.

Legha, W., Gaillard, S., Gascon, E., Malapert, P., Hocine, M., Alonso, S., & Moqrich, A. (2010). *stac1* and *stac2* Genes Define Discrete and Distinct Subsets of Dorsal Root Ganglia Neurons. *Gene Expression Patterns, 10*(7-8), 368-375.

Levanon, D., Bettoun, D., Harris-Cerruti, C., Woolf, E., Negreanu, V., Eilam, R.,…Groner, Y. (2002). The Runx3 Transcription Factor Regulates

Development and Survival of TrkC Dorsal Root Ganglia Neurons. *The EMBO Journal, 21*(13), 3454-3463.

Lionikas, A., Smith, C. J., Smith, T. L., Bünger, L., Banks, R. W., & Bewick, G. S. (2013). Analyses of Muscle Spindles in the soleus of Six Inbred Mouse Strains. *Journal of Anatomy, 223,* 289-296.

Maddox, F. N., Valeyev, A., Y., Poth, K., Holohean, A. M., Wood, P. M., Davidoff, R. A., Hackman, J. C., & Luetje, C. W. (2004). $GABA_A$ Receptor Subunit mRNA Expression in Cultured Embryonic and Adult Human Dorsal Root Ganglion Neurons. *Developmental Brain Research, 149,* 143-151.

Matthews, P. B. C. (1981). Evolving Views on the Internal Operation and Functional Role of the Muscle Spindle. *Journal of Physiology, 320,* 1-30.

Maxwell, D. J. & Bannatyne, B. A. (1983). Ultrastructural of Muscle Spindle Afferent Terminations in Lamina VI of the Cat Spinal Cord. *Brain Research, 288,* 297-301.

Mense, S. (2010). Functional Anatomy of Muscle: Muscle, Nociceptors and Afferent Fibers. In *Muscle Pain: Understanding the Mechanisms* (pp. 37-38). Berlin: Springer.

Milburn, A. (1973). The Early Development of Muscle Spindles in the Rat. *Journal of Cell Science, 12*, 175-195.

Moqrich, A., Earley, T. J., Watson, J., Andahazy, M., Backus, C., Martin-Zanca, D.,…Patapoutian, A. (2004). Expressing TrkC from the *TrkA* Locus Causes a Subset of Dorsal Root Ganglia Neurons to Switch Fate. *Nature Neuroscience, 7*(8), 812-818.

Nicholls, J. G., Martin, A. R., Fuchs, P. A., Brown, D. A., Diamond, M. E., & Weisblat, D. A. (2012). *From Neuron to Brain* (5th ed., pp. 280-281; 389-391). Sunderland: Sinauer.

Oliveira, L. (2010). Rat Muscle Opacity Decrease Due to the Osmosis of a Simple Mixture. *Journal of Biomedical Optics, 15*(5).

Patel, T. D., Kramer, I., Kucera, J., Niederkofler, V., Jessell, T. M., Arber, S., & Snider, W. D. (2003). Peripheral NT3 Signaling is Required for ETS Protein Expression and Central Patterning of Proprioceptive Sensory Afferents. *Neuron, 38,* 403-416.

Pierrot-Deseilligny, E. & Burke, D. (2012). *The Circuitry of the Human Spinal Cord: Spinal and Corticospinal Mechanisms of Movement.* Cambridge: Cambridge University Press.

Pritchett, D. B., Sontheimer, H., Shivers, B. D., Ymer, S., Kettenmann, H., Schofield, R., & Seeburg, P. H. (1989). Importance of a Novel GABAA Receptor Subunit for Benzodiazepine Pharmacology. *Nature, 338*(6216), 582-585.

Rudomin, P., & Schmidt, R. F. (1999). Presynaptic Inhibition in the Vertebrate Spinal Cord Revisited. *Experimental Brain Research, 129*, 1-37.

Schoultz, T. W. & Swett, J. E. (1972). The Fine Structure of the Golgi Tendon Organ. *Journal of Neurocytology, 1*(1), 1-26.

Scott, J. J. A. (2005). The Golgi Tendon Organ. In *Peripheral Neuropathy* (4th ed., Vol. 1, pp. 151-161). Philadelphia: Elsevier.

Sonner, P. M., & Ladle, D. R. (2013). Early Postnatal Development of GABAergic Presynaptic Inhibition of Ia Proprioceptive Afferent Connections in Mouse Spinal Cord. *Journal of Neurophysiology, 109*, 2118-2128.

Stacey, M. J. (1969). Free Nerve Endings in Skeletal Muscle of the Cat. *Journal of Anatomy, 105,* 231-254.

Steffens, H., Dibaj, P., & Schomburg, E. D. (2012). In Vivo Measurement of Conduction Velocities in Afferent and Efferent Nerve Fibre Groups in Mice. *Physiological Research, 61,* 203-214.

Sun, Y., Dykes, I. M., Liang, X., Eng, S. R., Evans, S. M., & Turner, E. (2008). A Central Role for Islet1 in Sensory Neuron Development Linking Sensory and Spinal Gene Regulatory Programs. *Nature Neuroscience, 11*(11), 1283-1293.

Sürmeli, G., Akay, T., Ippolito, G. C., Tucker, P. W., & Jessell, T. M. (2011). Patterns of Spinal Sensory-Motor Connectivity Prescribed by a Dorsoventral Positional Template. *Cell, 147,* 653-665.

Suzuki, H., Kawai, J., Taga, C., Yaoi, T., Hara, A., Hirose, K., Hayashizaki, Y., & Watanabe, S. (1996). Stac, a Novel Neuron-Specific Protein with Cysteine-Rich and SH3 Domains. *Biochemical and Biophysical Research Communications, 229,* 902-909.

Tourtellotte, W. G., Keller-Peck, C., Milbrandt, J., & Kucera, J. (2001). The Transcription Factor Egr3 Modulates Sensory Axon-Myotube Interactions during Muscle Spindle Morphogenesis. *Developmental Biology, 232,* 388-399.

Vult von Steyern, F., Martinov, V., Rabben, I., Njå, A., de Lapeyrière, O., & Lømo, T. (1999). The Homeodomain Transcription Factors Islet 1 and HB9 are Expressed in Adult Alpha and Gamma Motoneurons Identified by Selective Retrograde Tracing. *European Journal of Neuroscience, 11,* 2093-2102.

Wright, D. E., Zhou, L., Kucera, J., & Snider, W. D. (1997). Neuron Introduction of a Neurotrophin-3 Transgene into Muscle Selectively Rescues Proprioceptive Neurons in Mice Lacking Endogenous Neurotrophin-3. *Neuron, 19,* 503-517.

Wu, M., Deng, L., Zhu, G., & Li, Y. (2010). G Protein and its Signaling Pathway in Bone Development and Disease. *Frontiers in Bioscience*, *15*, 957-985.

Wu, S., Koshimizu, Y., Feng, Y., Okamoto, K., Fujiyama, F., Hioki, H.,…Mizuno, N. (2004). Vesicular Glutamate transporter Immunoreactivity in the Central and Peripheral Endings of Muscle-Spindle Afferents. *Brain Research, 1011*(2), 247-251.

Zelená, J. (1994). *Nerves and Mechanoreceptors: the Role of Innervation in the Development and Maintenance of Mammalian Mechanoreceptors.* London: Chapman & Hall.

Zurborg, S., Piszczed, A., Martínez, C., Hublitz, P., Banchaabouchi, M. A., Moreira, P., Perlas, E., & Heppenstall, P. A. (2011). Generation and Characterization of an *Advillin*-Cre Driver Mouse Line. *Molecular Pain*, *7*(66), 1-10.